TALLINN UNIVERSITY OF TECHNOLOGY
SCHOOL OF ENGINEERING

Department of Materials and Environmental Technologies

SIMULATIONS OF BUILDING INTEGRATED PHOTOVOLTAIC THERMAL FOOD DEHYDRATOR WITH HEAT RECOVERY

EHITISINTEGREERITUD PÄIKESEPANEELIDE BAASIL TOIMIVA TOIDUAINETE KUIVATI TEOSTATAVUSE TEOREETILINE ANALÜÜS

MASTER THESIS

Student Iryna Yakobiuk

Student code 156324KAYM

Supervisor Andri Jagomägi, PhD, Research Scientist

Tallinn, 2017

AUTHOR'S DECLARATION

Hereby I declare, that I have written this thesis independently.
No academic degree has been applied for based on this material.
All works, major viewpoints and data of the other authors used in this thesis have been referenced.

"....." 2017

Author: .....

/signature /

Thesis is in accordance with terms and requirements

"....." 2017

Supervisor: ….....

/signature/

Accepted for defence

"....."....."2017

Chairman of theses defence commission: .....

/name and signature/

TALLINNA TEHNIKAÜLIKOOL
INSENERITEADUSKOND

Materjali ja keskkonnatehnoloogia instituut

EHITISINTEGREERITUD PÄIKESEPANEELIDE BAASIL TOIMIVA TOIDUAINETE KUIVATI TEOSTATAVUSE TEOREETILINE ANALÜÜS

SIMULATIONS OF BUILDING INTEGRATED PHOTOVOLTAIC-THERMAL FOOD DEHYDRATOR WITH HEAT RECOVERY

MAGISTRITÖÖ

Üliõpilane: Iryna Yakobiuk

Üliõpilaskood: 156324KAYM

Juhendaja: Andri Jagomägi, PhD, Teadur

Tallinn, 2017.a.

AUTORIDEKLARATSIOON

Olen koostanud lõputöö iseseisvalt.
Lõputöö alusel ei ole varem kutse- või teaduskraadi või inseneridiplomit taotletud.Kõik töö koostamisel kasutatud teiste autorite tööd, olulised seisukohad, kirjandusallikatest ja mujalt pärinevad andmed on viidatud.

“.....” 2017

Autor: .....

/ allkiri /

Töö vastab bakalaureusetöö/magistritööle esitatud nõuetele

“.....” 2017

Juhendaja: .....

/ allkiri /

Kaitsmisele lubatud

“.....”.....2017

Kaitsmiskomisjoni esimees .....

/ nimi ja allkiri /

Table of Contents

Abbreviations and Acronyms

Symbol	Description	SI Unit
Ah	absolute humidity	g/m^3
C_0, K_0	coefficients fitted by regression analysis.	
c	heat capacity of the air	$kJ/(kg \cdot K)$
d_p	particle dimension	m
E_{bat}	charge level of the battery	kWh
$E_{bat.max}$	maximum electrical capacity of the batteries	kWh
F_0,F_1	coefficients for crystalline silicon cells	
G	irradiance level	W/m^2
ΔH_C	water heat of sorption (mono and multi molecular layers)	
ΔH_K	water vapor heat of condensation	
i	hour number index	
j	tray number index	
k_0	the empirical coefficient estimated by fitting regression	h^{-1}
k_1, k_2, k_3, k_4	the empirical coefficients estimated by fitting regression	
k_M	drying constant	h^{-1}
L	latent heat of the water	kJ/kg
m	total number of trays	
M	molecular weight of water	g/mol
$\dot{m}_a$	air mass flow rate	kg/h
$\dot{m}_{ev}$	moisture evaporation rate	kg/h
m_w	actual water mass in the air	gram
n	total number of hours	
P_C	power consumed by system	kW
P_{heater}	heater power	kW
P_{max}	maximum power of the module in standard conditions	kW
P_{mod}	PV output power	kWh
P_{PV}	power produced by photovoltaic modules	kW
p_S	saturated vapor pressure	hPa
Q_{ev}	energy needed for moisture evaporation	kJ

Q_{losses}	heat losses through the walls	kJ
R	ideal gas constant	$\frac{m^3 hPa}{mol \cdot K}$
Rh	relative humidity	%
t	temperature	˚C
t_{mod}	temperature of the modules	˚C
$t_{s.p.}$	set point temperature	˚C
V	air volume	m^3
x	material thickness	mm
X_S	material moisture content	kg/kg db
X_{SE}	equilibrium material moisture content	kg/kg db
α	absorption	
α_{PV}	PV cell absorption	
γ	temperature coefficient of maximum power	
δ	material layer thickness	m
ε	Emissivity	
k	thermal conductivity	W/(m*K)
λ	heat conductivity	W/(m·K)
ρ	material density	kg/m^3
τ	Time	hour
τ_{gl}	glass transmittance	
ϑ	air velocity	m/s

PV – photovoltaic

PVT – photovoltaic thermal

BIPVT – building integrated photovoltaic thermal

COP – coefficient of performance

1. Introduction

Many recent studies have focused on photovoltaic thermal (PVT) technology. It is considered to be one of the most promising technologies to produce on-site electricity and heat energy directly from the sun. PVT system consists of the two parts: photovoltaic system that converts solar energy into electricity and thermal system that converts solar energy into thermal energy. Furthermore, the application of PVT collectors reduces the temperature of the PV cells and therefore increases the electricity production efficiency.

Thermal energy from the hybrid collectors can be utilized in various application. One possibility of using heat from the PVT channel is food drying. Latter is one of the most popular methods of food preservation that is useful for the reduction of the food spoilage. It also helps to reduce the weight and volume of the product for easier transportation and storage. In addition, farmers use dryers during the harvest when there is large amount of agricultural products and price for product drops down significantly. Nowadays most of dryers work on electricity, diesel or other fossil fuels and have negative effect on environment. In addition, fossils have high prices. Therefore, it is reasonable to look for alternative energy sources as conversion of solar irradiance into heat and electricity by building integrated photovoltaic thermal (BIPVT) collectors.

The main advantages of BIPVT technology in food dehydration are:

- the period of the high radiation intensity matches with the harvesting period;
- it reduces consumption of fossil fuels;
- the simplicity of technology. Heated air is essential for dehydration and air type BIPVT
- collectors are simple to produce;
- replaces parts of building and therefore reduces the cost for construction.

However, the main problem in solar drying is solar radiation intermittence. Therefore, such a drying system should have some backup energy source (batteries, grid electricity etc.). Feasibility of such a system should be investigated.

The aim of this study is to simulate the performance of a solar drying system based on air type BIPVT collectors in the Estonian climate for period from the 1st of June to the 30th of September for different set point temperatures in the drying chamber; to simulate amount of the apples to be dried depending on the drying chamber configurations, air flow directions and different set point temperatures in the drying chamber.

2. Literature review

2.1. Photovoltaic thermal technology

A significant amount of research work has been conducted on the PVT technology in the last 40 years that have shown a gradual increase in their development. The schematic of the PVT technologies are presented on the Figure 1. There are alternative approaches in PVT integration, such as PVT/air, PVT/water and PVT concentrated collector [1]. Tushar and Dhoble [2] have formed other classification based on heat transfer technology and integration PVT system that is shown in Figure 2.

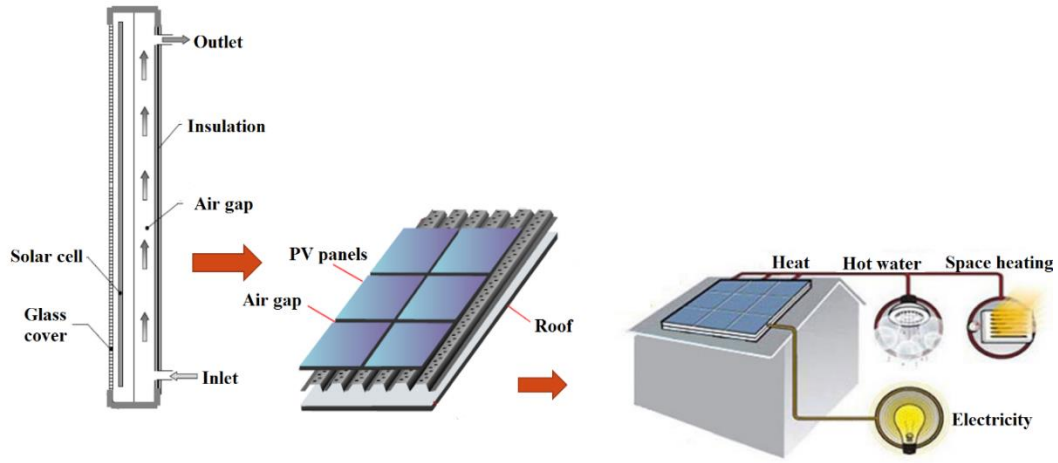

Figure 1. Schematic of various solar technologies [3]

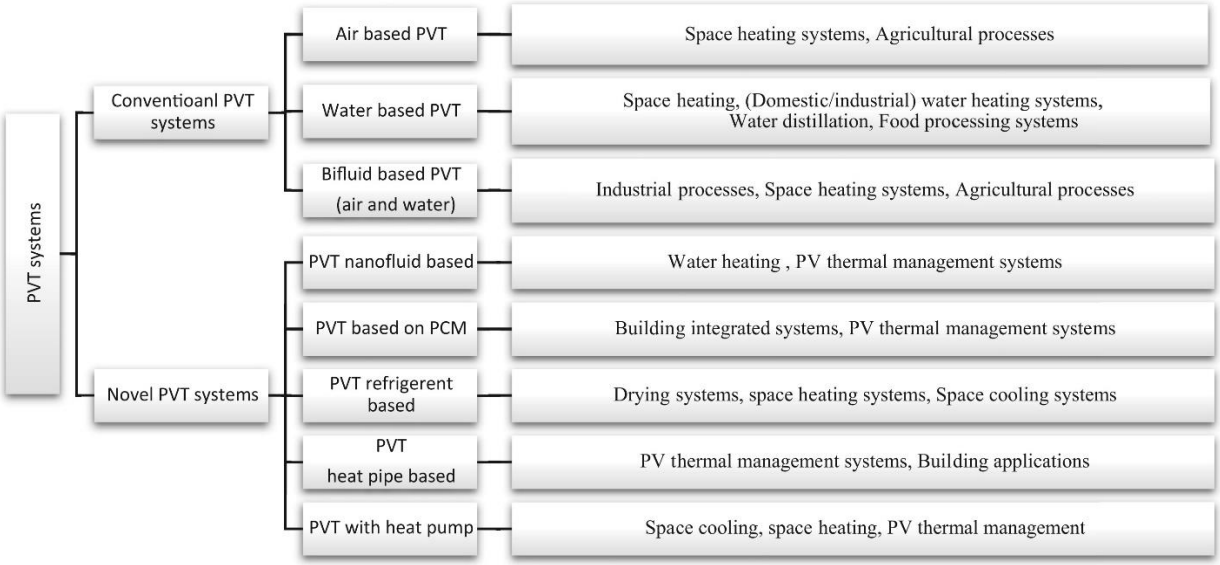

Figure 2. Classification of PVT system [2]

Tripanagnostopoulos et al. [4] have investigated a hybrid solar system and presented the outdoor test results. Their research has shown that PV cooling increases the electrical efficiency of PV panels. Consequently, increasing the total energy output of the system. Kemmoku et al. [5] have found that for concentrated PV system the electrical efficiency decreases about 0.3% with temperature rises by 1˚C.

PVT system consists of PV panels and thermal collectors. According to [6] - [7], the advantages of hybrid thermal system compare with separate PV and thermal system are following:

- PVT system occupies less area than PV panels and thermal collectors separately;
- PVT system is cheaper because it requires less material;
- Fluid temperature is higher in PVT system than in thermal collector;
- Overall efficiency is higher in the hybrid system than in separate one.

Huide et al. [8] has tested three types of solar utilization technologies including PV panels, PVT panels, and solar collectors equipped with monitoring devices. The thermal efficiency of the solar collectors is higher than in PVT system. But the electrical efficiency in PVT is higher comparing with the PV modules. The results of the test are presented in Table 1.

Table 1. Electrical and thermal efficiency of the Solar collectors, PV and PVT modules [8]

Type of the system	Electrical efficiency, %	Thermal efficiency, %
Solar Collectors	-	67.8
PV modules	11	-
PVT modules	12.7	51.3

Hajiji M. et al. [9] have developed a numerical method that allows finding the temperatures of PVT panel for each layer. Furthermore, they have been investigated the effect of the mass flow rate on the electrical efficiency of the system. Solanki et al. [10] have installed a PV/T solar heater system in order to measure dependent factors by changing the mass flow rate of air and solar intensity in steady state conditions. They have figured out that the air temperature increases heat transfer from PV module and hence efficiency decreases. It is shown in Figure 3.

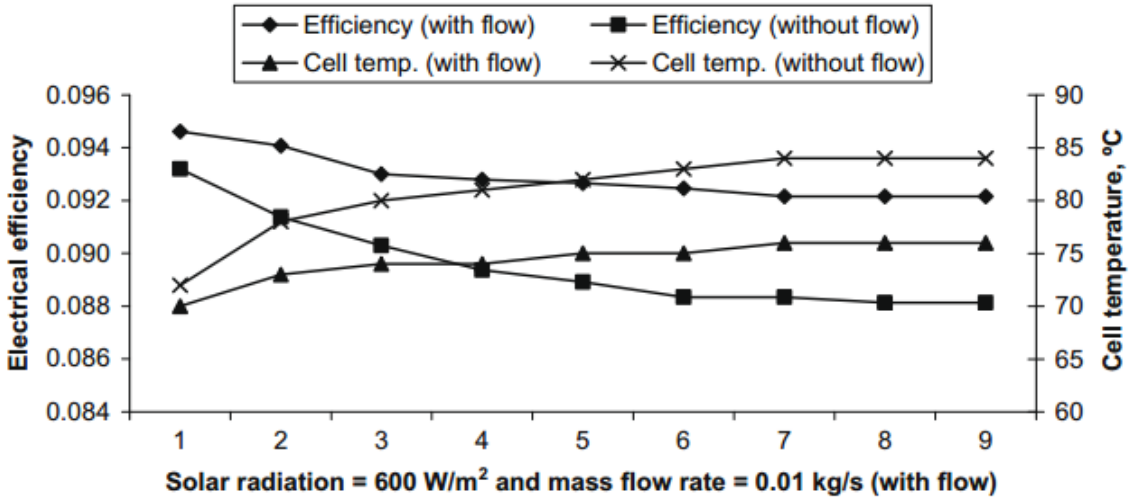

Figure 3. The electrical efficiency and cell temperature with/without flow [10]

The principle of using PVT system depends on the working fluid. PVT air collectors are less expensive and easier to construct compared to water-based PVT. The basic application of PVT air systems is space heating and agriculture products drying [11].

The general progress in BIPVT air applications have been reviewed by several investigators, including Hachem et al. [12] who have presented a study of thermal and electrical efficiency from BPVT for different roofs and Vats and Tiwari [13] have analyzed the indoor air parameters with BIPVT.

In order to estimate heat transfer and losses in the cavity of the BIPVT Zogou and Stapountzis [14] have used CFD (Computational Fluid Dynamics) simulation for airflow inside a testing device. As a result, they have figured out that the heat transfer between the fluid and PV panel is better with increasing the mass flow rate. However, increasing flow rate requires additional energy from the fan. It is essential to provide optimal point when additional energy for the fan does not exceed the produces heat energy. Charalambous et al. [15], Daghigh et al. [16] have presented the mathematical model for required fluid speed. Furthermore, Bambrook and Sproul [17] have used a TRNSYS simulation analysis in order to determine appropriate airflow to gain the best efficiencies. On the other hand, the PVT system can be tested with The PASSYS test cell (Passive Solar Components and Systems Testing) [18]. Crick F. et al. [19] have constructed a prototype ventilated PV façade. As a result, the optimum airflow rate with irradiance level 80 W/m^2 was 0.04 m/s and for 650 W/m^2 was 0.15 m/s.

2.2. Working principles and types of solar dryers

2.2.1. Open solar drying

The open solar drying process is the simplest and cheapest way of the solar drying. The product is placed in the open air and the moisture evaporated by the effect of the solar radiation and natural air ventilation. The process does not require electricity or fuel. In spite of these positive aspects, there are many disadvantages of such type of drying:

- open to contamination by dust, microbes and animals;
- completely dependent on the weather conditions;
- very slow drying rates with the danger of mold growth;
- time in between drying sessions allows the growth of unwanted microorganisms;

Figure 4 depicts the process of the drying under the open sun. There are series of losses such as conductive losses, high convective and evaporated heat losses, short and long wavelength radiation losses.

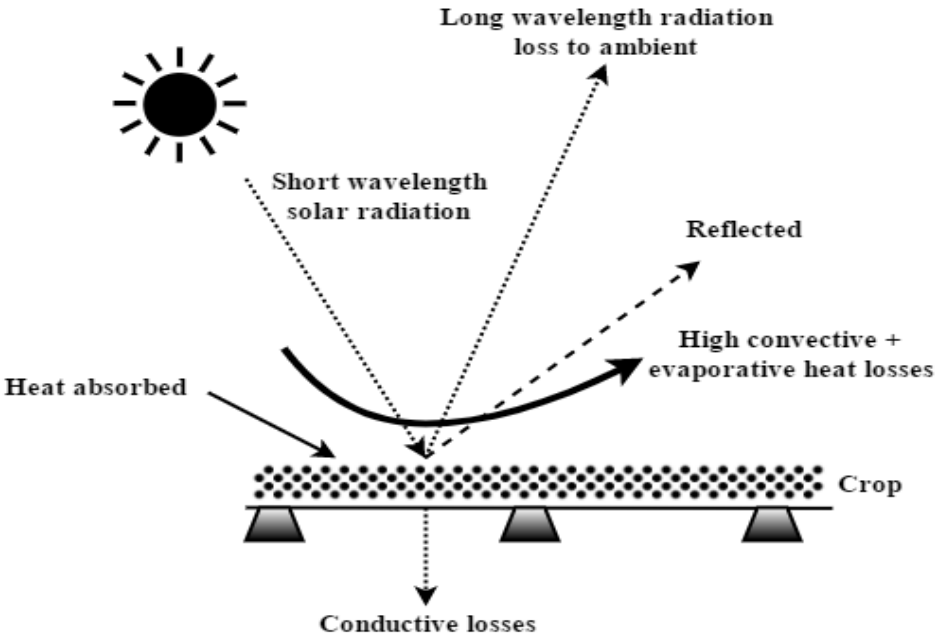

Figure 4. Principle of the open-air crop drying [20]

2.2.2. Direct solar drying / solar cabinet dryer

Direct solar dryers designed as a cabin covered with transparent material and use only the natural movement of heated air. Figure 5 shows schematics of direct solar drying. Some amount of solar radiation passes through the transparent cover and absorbed by the product and the other reflects back to the atmosphere.

The advantages of such type of dryer over the open solar drying process are as follows:

- Protection from the rain, dust, dews, insects, debris etc.
- It can reach higher temperatures because of the limitation of the natural air movement.

However, the direct solar drying has some disadvantages:

- Poor vapor removal that causes slow drying rate.
- Capacity limitation. The layer of the product on the trays should be relatively thin in order to allow all the product be dried at the same time.
- Moisture condensation on the cover reduces its transmissivity.

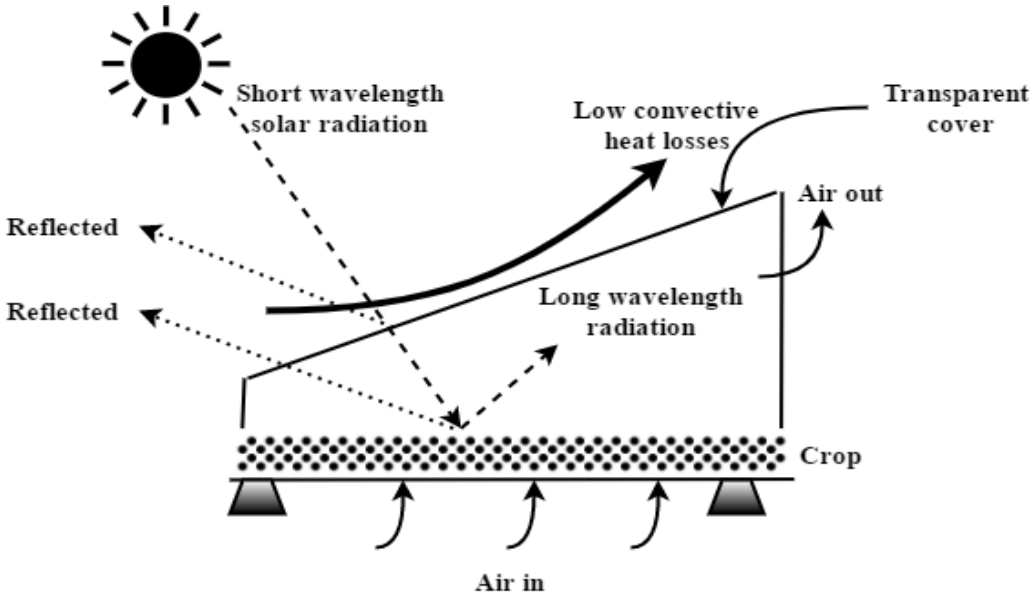

Figure 5. Principle of solar cabinet dryer [20]

2.2.3. Indirect solar drying

Both previous types of solar dryers are directly dependent on the availability of the sun and it reduces their functionality. To overcome instability during off shining periods the new types of technologies have been developed. The main requirements in the development of indirect solar dryers are as follows:

- Continuous drying process;
- Easy to manufacture and easy to operate;
- Maximum use of solar energy;
- Control system over rate of drying;
- The system has to be financially attractive.

Figure 6 shows working principle of indirect solar dryer.

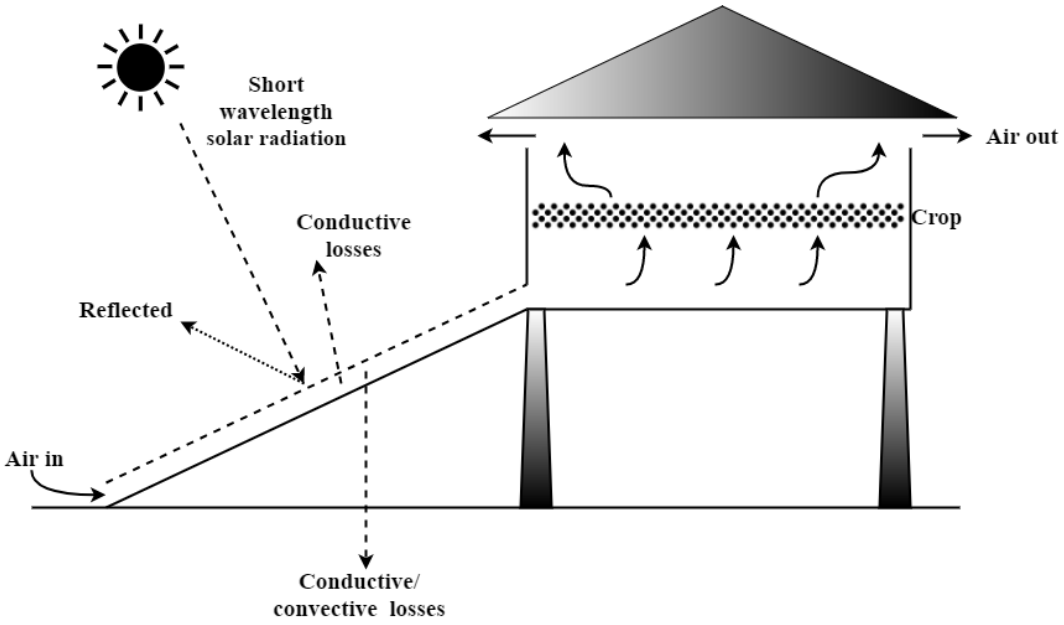

Figure 6. Principle of the indirect solar dryer [20]

Figure *7* explains the classification of solar dryers [21]. Solar dryer is designed to the quantity, characteristics and designation of the product to be dried and the energy source that is included in the system.

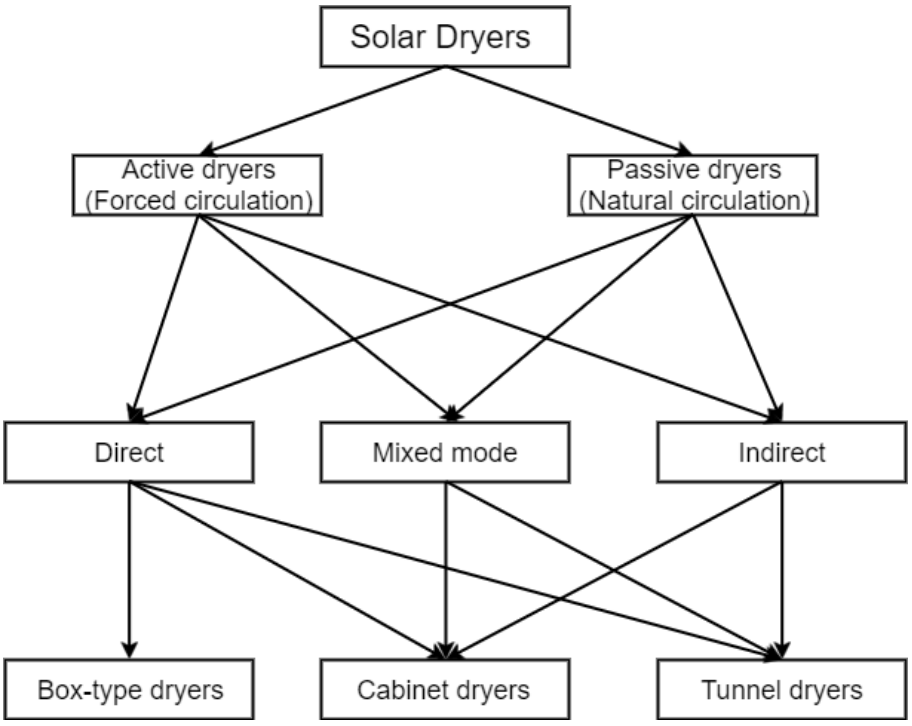

Figure 7. Classification of the dryers over the mode of air circulation [21]

2.3. Photovoltaic thermal solar dryers

One of the inventive methods of using building integrated photovoltaic is the photovoltaic thermal air collector or hybrid solar collector, which converts solar radiation into both thermal and electrical energies for use in drying systems.

Solar radiation is used for drying purpose all over the world. The drying process under the open sun is the cheapest method of the water evaporation but it has numerous disadvantages and the main is the bacterial influence. The usual dryers consume a large amount of the fuel and the process became more expensive but faster and more effective. Last decades with popularization renewable energy sources solar collectors, PV panels and PVT panels found their application in the drying process. Moreover, dryer with PVT panels can be used without additional energy consumption. However, the weather conditions have to be taken into account. In case of installing PVT panels, it is expedient to have several modes during the system operations.

In the paper by Farkas [22], the modular solar dryer is depicted in Figure 8. Presented dryer can have different modes:

- ventilation of ambient air is natural;
- artificial ventilation using the electrical fan when the PV module is applied;
- artificial ventilation using preheated air from the collector;
- the combination of above modes can be used.

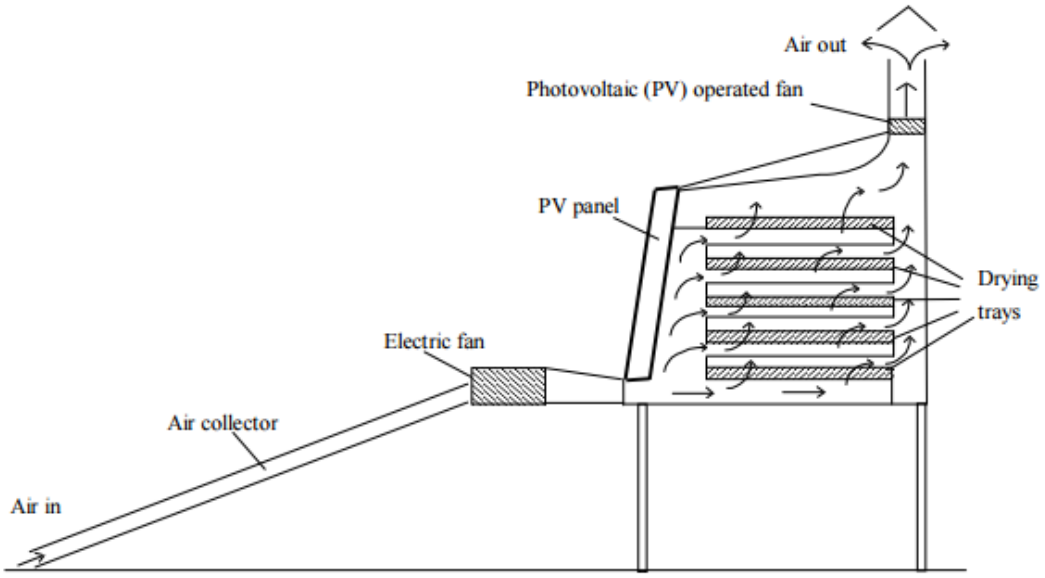

Figure 8. Scheme of the modular solar dryer [22].

Hamid et al. [23] have made an investigation on a hybrid photovoltaic–thermal solar dryer equipped with a heat pump system for saffron drying, in order to obtain a high-quality product and reduce fossil fuel consumption. They have analyzed the effect of air mass flow rate, drying air temperature and two different drying modes (with and without heat pump). On Figure 9 is shown the dryer that consists of the PVT solar collectors and heat pump.

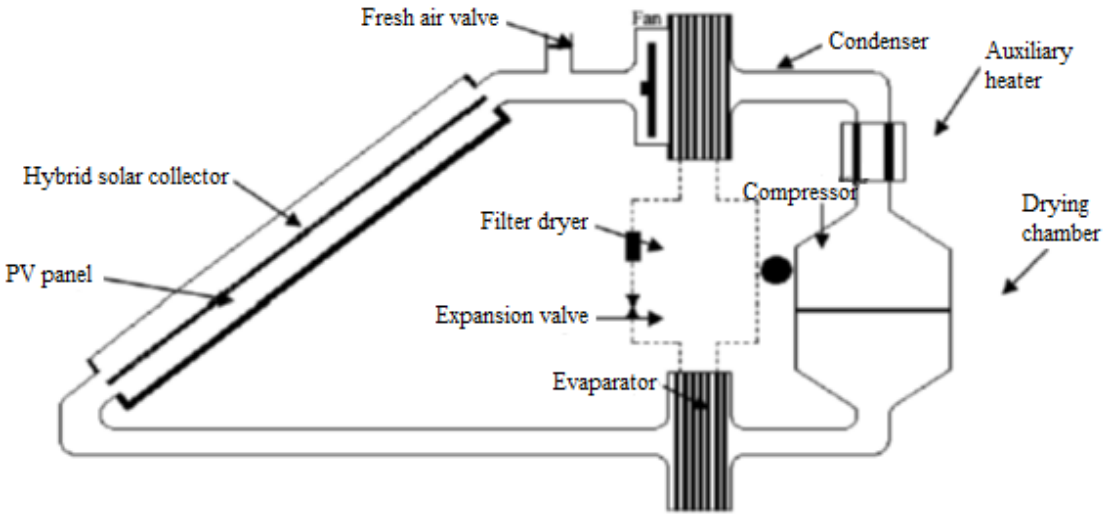

Figure 9. Schematic representation of the dryer with PVT and heat pump unit [23].

They have figured out that with increasing the airflow rate and temperature the drying time decreases. In addition, according to this report heat pump reduces the energy consumption by 33%.

Nayak et al. [24] have designed the off-grid dryer for utilizing forced air circulation using photovoltaic thermal panels. They have conducted the measurement of the temperature of the output air from the PVT channel and the temperature of the air in each tray. In addition, researchers have shown the results of techno-economic analysis of hybrid PVT solar dryer of cauliflower. As a result, PV solar dryer can be self-sustained and the payback period is less than expected life of the dryer.

Mortezapour et al. [25] have compared of two types of hybrid PVT solar collectors. The PVT with glass to glass and glass to tedlar solar collectors were developed. The glass-to-glass solar collectors gave better thermal efficiency and glass to tedlar is better for electrical performance. Finally, after mathematical calculation, it was defined that the overall thermal efficiency of glass to tedlar PV module was more than the overall efficiency of glass-to-glass PV module.

2.4. Methodologies of drying process simulation

Mass flow rate and the temperature of the air are the most important parameters that indicated the quality of the dried product. There are also other parameters such as sample thickness, velocity, final moisture content and humidity of the air [26].

The basic idea of modeling the drying kinetics of some fruits and vegetables is to decide the optimal drying conditions, to analyze the drying process and to estimate needed energy [27]. The drying kinetics depend on the type of dryer, the drying conditions and the characteristics of the material to be dried. The drying process can be predicted using suitable thin-layer models that involves at the same time heat and mass transfer operations.

Thin-layer drying models can be classified as theoretical, semi-theoretical and empirical models. The empirical and semi-theoretical models are similar. The main challenges faced by the empirical models are that they depend largely on experimental data and provide limited information about the heat and mass transfer during the drying process [28].

Meisamiasl et al. [29] have compared different mathematical models, such as logarithmic [30], Henderson and Pabis [31], Hii model [32], Midilli model [33], and have selected the most proper for thin-layer drying of apples. According to results, the Henderson and Pabis model has given the best results. All reviewed models require experimental data for feeding equations.

There are a huge variety of the mathematical models for prediction drying kinetics of agricultural and food products. Unfortunately, none of these models fit well for a wide range of drying conditions and products. In order to get better results Aghbashlo et al. [34] have created a new model and fed it with experimental data that were taken from the carrot drying process. Furthermore, the new method in comparison with others gave better results.

Suitability of each model depends on the type of the product, the size of the slides, the temperature and velocity of the air. For this paper, all the models for apples have been investigated. Akpinar [35] have calculated the kinetic model for apples with the slide sizes 8*8*18 mm, temperature varied from 60 to 80˚C and air velocity from 1 to 1.5 m/s. Zarein et al. [36] have used the apples with 3*7 mm size and drying parameters were temperature 50-95 ˚C and constant air velocity 1 m/s. Meisamiasl et al. [37] had apple slides 2*6 mm, the temperature in the drying chamber from 40 to 80 ˚C and air velocity 0,5 m/s. Results of thin layer modeling of apples slices with different parameters showed that the Midilli et al. [33] model is more suitable for drying kinetics calculations. Midilli model is a modification of the existing Henderson and Pabis model. This model is suitable for wide range of the product type.

Timoumi et al. [38] published a paper about simulation model for apples drying. They studied that the temperature parameter (Figure 10) dominated by airflow rate (Figure 11) or humidity range (Figure 12) for drying kinetic simulations.

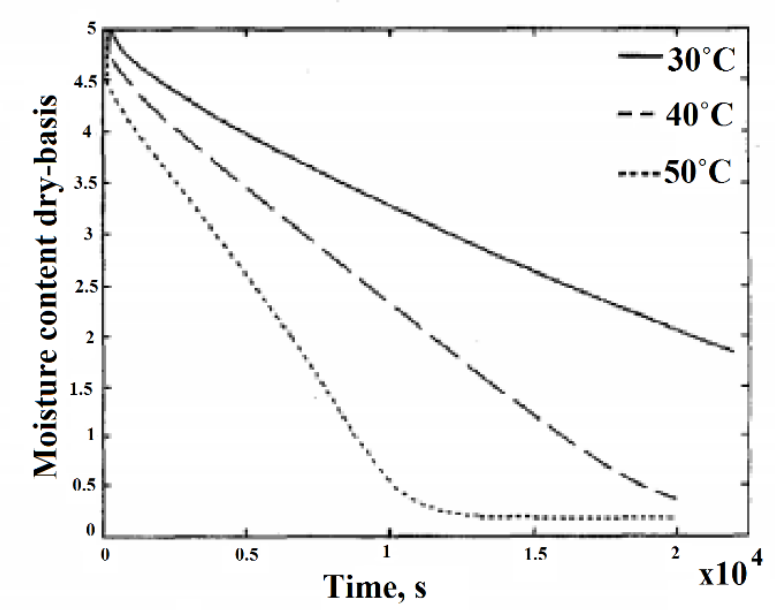

Figure 10. Temperature dependence in the evaporation process [38].

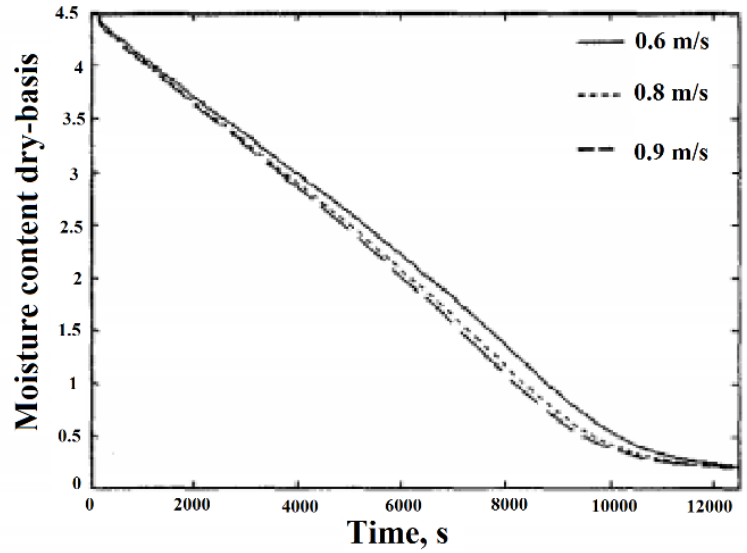

Figure 11. Air velocity dependence in the evaporation process [38].

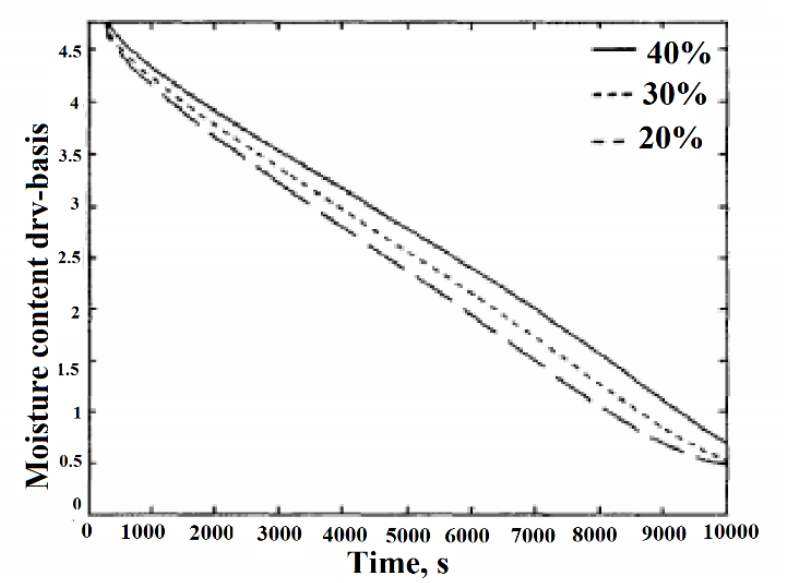

Figure 12. Humidity dependence in the evaporation process [38].

3. Simulation methodology of building integrated photovoltaic thermal dryer

3.1. Description of theoretical object

The theoretical object under investigation is a farmhouse with built in food dehydration system. The farmhouse is equipped with air type BIPVT collectors that are basically standing seam metal sheet integrated PV cells with the organized air gap (PVT channel) under the back sheet of PV modules. The fan forces the air movement and therefore the air is heated as it is shown in Figure 13. The roof has the area of 70 m^2 with the nominal PV power of 9 kW.

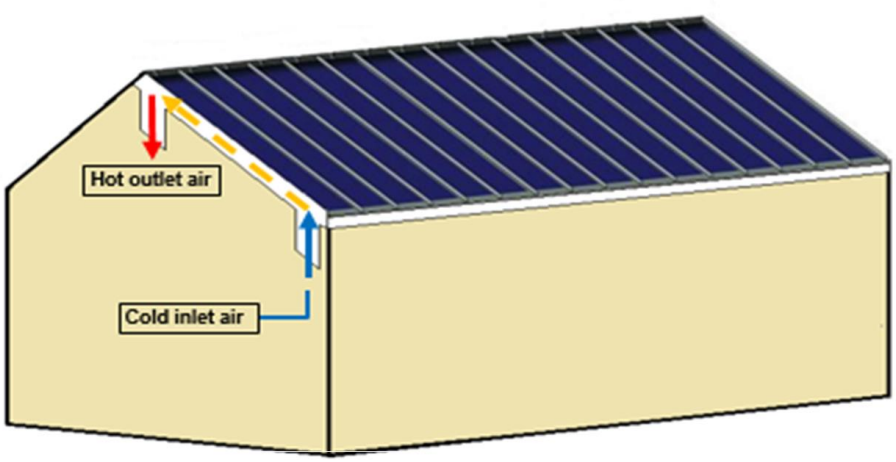

Figure 13. Working principle of BIPVT collectors

Apart from the fan and BIPVT collectors, the system contains:

- the drying chamber to place apples to be dried;
- the electrical heater for auxiliary heating, when the production of heat from PVT channel is not high enough;
- the heat recovery unit (HRU);
- the batteries to increase self-consumption.

Figure 14 shows the relations between system's elements. BIPVT collectors produce electricity and heat in form of hot air. Hot air is used for drying of apples. Electricity goes for the supply of the fan, the heater and controlling device. Whenever it is possible, the fan and the heater operate on the PV or battery power. If there is surplus of electricity production from PV

panels, it is used to charge the batteries. In addition, the system is connected to the electrical grid in order to provide continuous 24/7 drying and backup power.

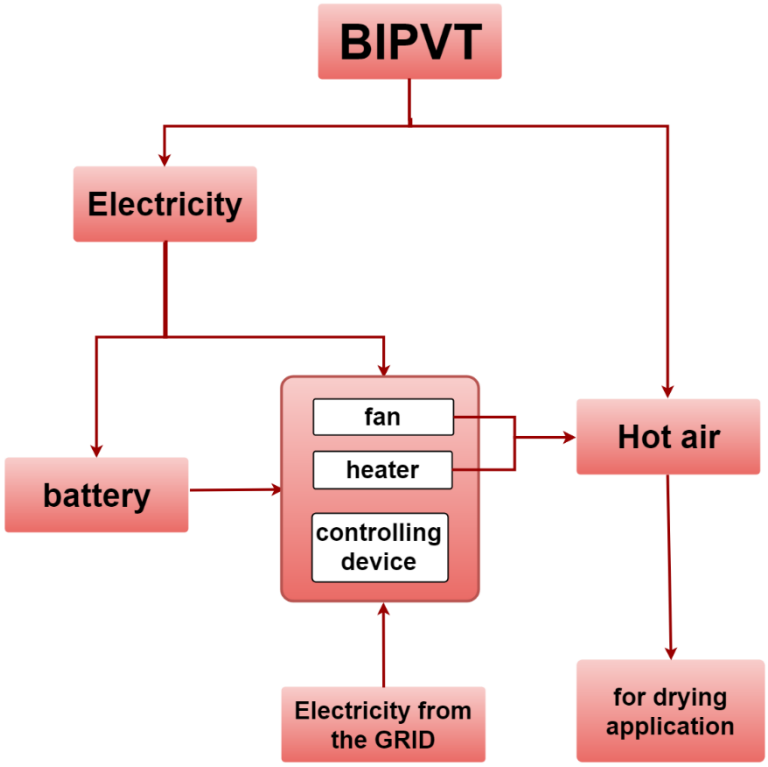

Figure 14. Schematic description of the working principle of the food dehydrator.

There are two operational modes in the drying system. The Figure 15. Schematic of the dryer with one-directional shows schematics of modes. In both cases, fresh air is taken from the outside and preheated by HRU by exhaust air from drying chamber. The system operates in the first mode when the solar irradiance is available and BIPVT collectors can heat the air after HRU. So after HRU, the air is heated by BIPVT collectors and if the temperature is still not high enough it is heated again by the electrical heater, directed to the drying chamber and released through the HRU. The system operates in the second mode during the night or when BIPVT collectors cannot heat the air up. Therefore, the air bypasses BIPVT collectors. In this case, the main source of heat is the electrical heater.

In the drying chamber, we assumed to use trays made of stainless steel wire mesh. The chamber's walls built of extruded polystyrene and plywood. The air is supposed to go through the trays. In present work, one-directional and bidirectional air flows through the drying chamber were investigated. Air flow direction affects the most important parameters for drying rate on each tray: average relative humidity and average temperature.

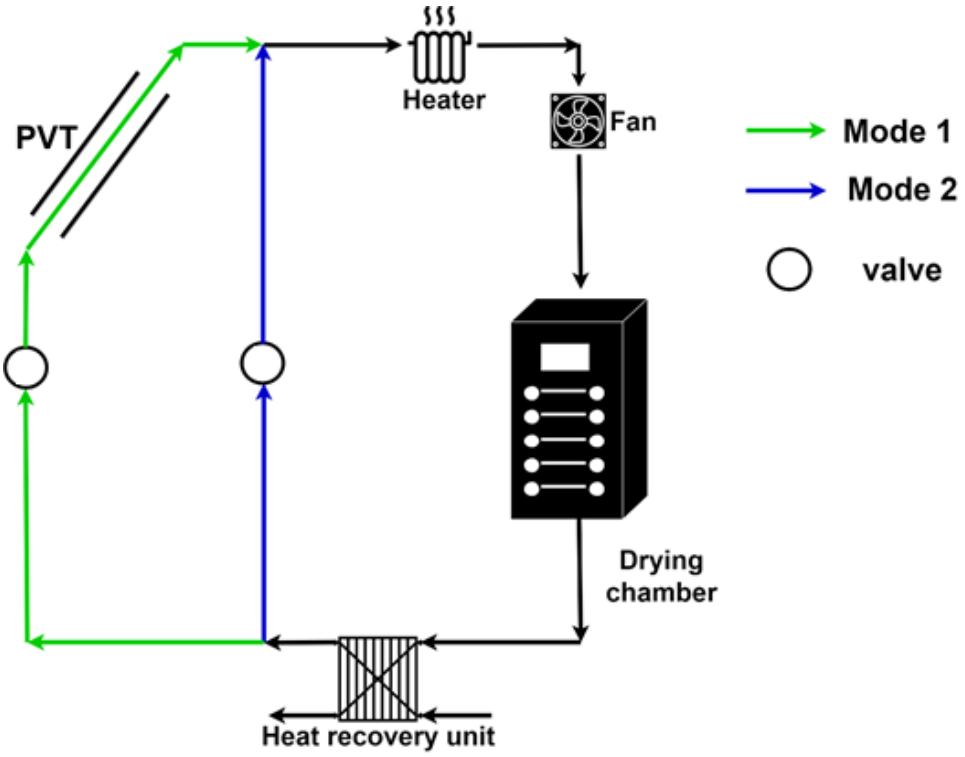

Figure 15. Schematic of the dryer with one-directional air flow

Figure 15 shows schematically the drying system with one-directional air flow through the drying chamber. One-directional air flow means that system does not change air flow direction through the drying chamber with time at all. Figure 16 (a) shows the gradient of the temperature and humidity in the drying chamber for one-directional flow that are caused by heat losses and additional evaporations. The first extreme point of this gradient is at the inlet of drying chamber where the air has the highest temperature and the lowest humidity. The second is at the outlet of drying chamber. As a result, the dehydration rate of product on the first and last tray is very different. In this case, it is complicated to organize at least approximately similar drying rate of the product on all trays. There is no possibility to dry trays by batches. Thus, it requires a lot of attention since someone needs to replace trays with dry product by raw one often. In addition, this causes some heat losses during opening the door and takes some time to stabilize the temperature regime in the chamber. With one-directional drying it is also complicated to control the process of each tray separately. Each dried tray should be replaced by one with raw product in time, because over-dried product will be brittle and unsuitable for use.

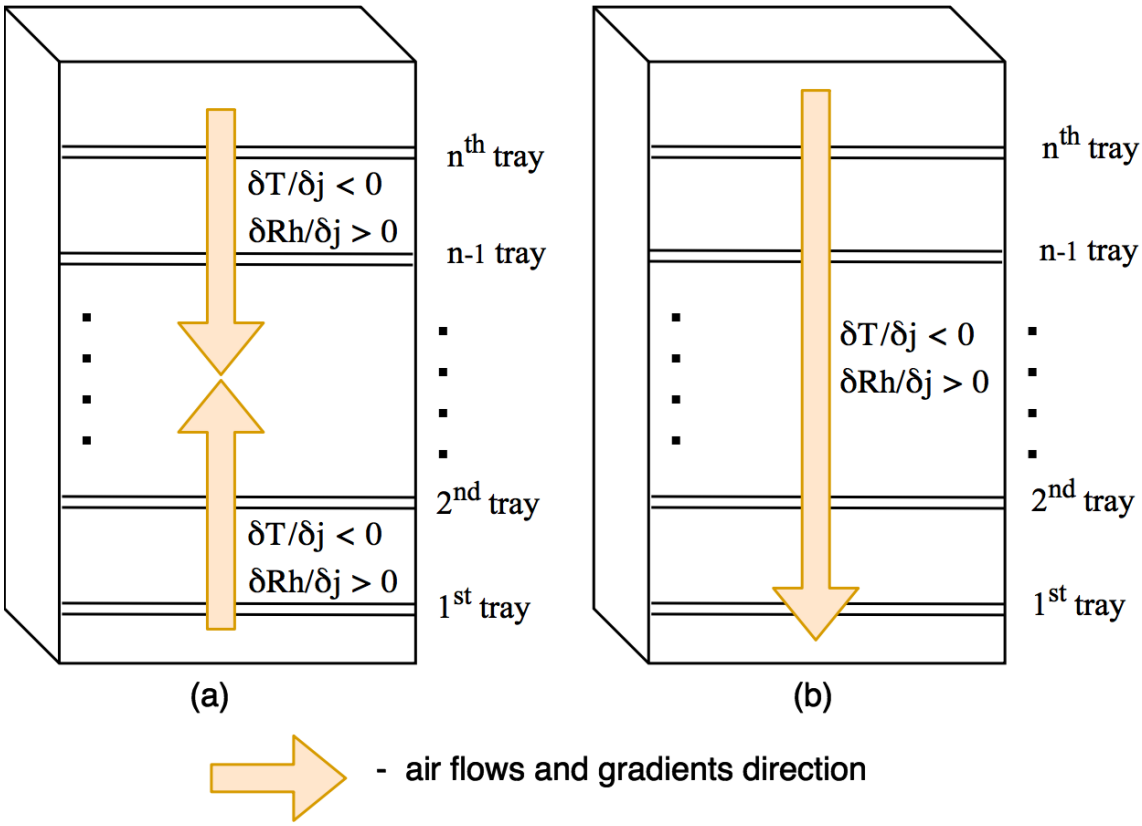

Figure 16. Schematic representation of the gradients of the average temperature and average relative humidity in the drying chamber with (a) one-directional and (b) bidirectional air flows: *T* is average temperature, *Rh* is average relative humidity, *j* – tray number, *n* – number of trays in stack

Bidirectional air flow is air flow through the drying chamber that changes its direction each hour. Therefore, the average temperature and relative humidity on the levels of different trays are more equalized. In this case the first extreme point of the gradient is at the inlet and the outlet of drying chamber. The second point is in the middle. Thus, bidirectional airflow balances drying rate of all trays. The product on all trays would be ready approximately at the same time and it makes possible dehydration of the trays by the batches. In addition, it allows using load sensors for controlling the process. Being familiar with initial weigh of the product and needed final moisture content it is possible to calculate the final weigh of the product and stop the system at this point. The only disadvantage of bidirectional airflow comparing with one-directional is additional piping and dampers.

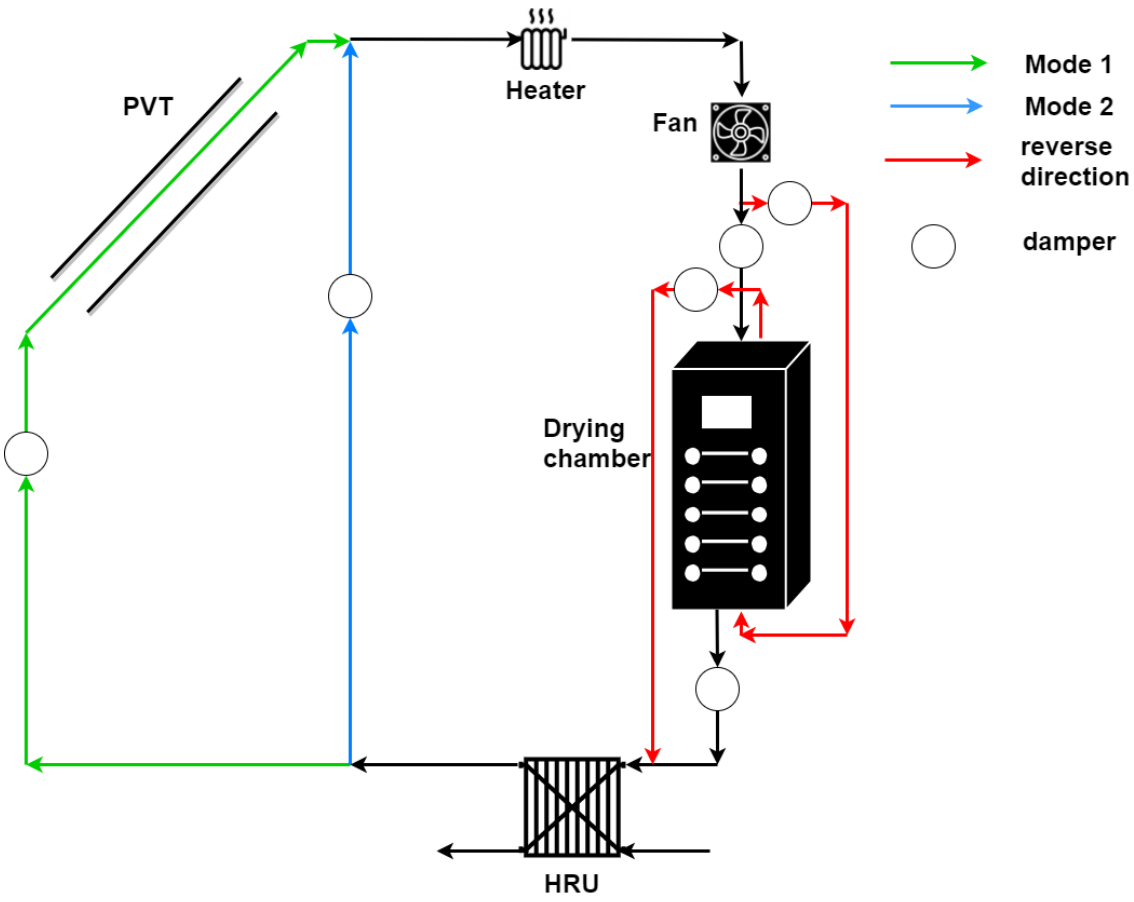

Figure 17. Schematic of the dryer with bidirectional air flow

3.2. Simulation of outlet air parameters from the PVT channel

The simulations were conducted based on the dynamical thermal model of an air type PVT system that is described in Ref [39]. From the simulation, the hourly temperature of air and air flowrate into the drying chamber were generated.

As it is shown in the Figure 18, there are convection in the front side, backside and in the air channel that mostly depends on the outside temperature and wind speed. In addition, the infrared (IR) radiation heat exchange, solar radiation and PV current influence on the heat balance of PVT air system.

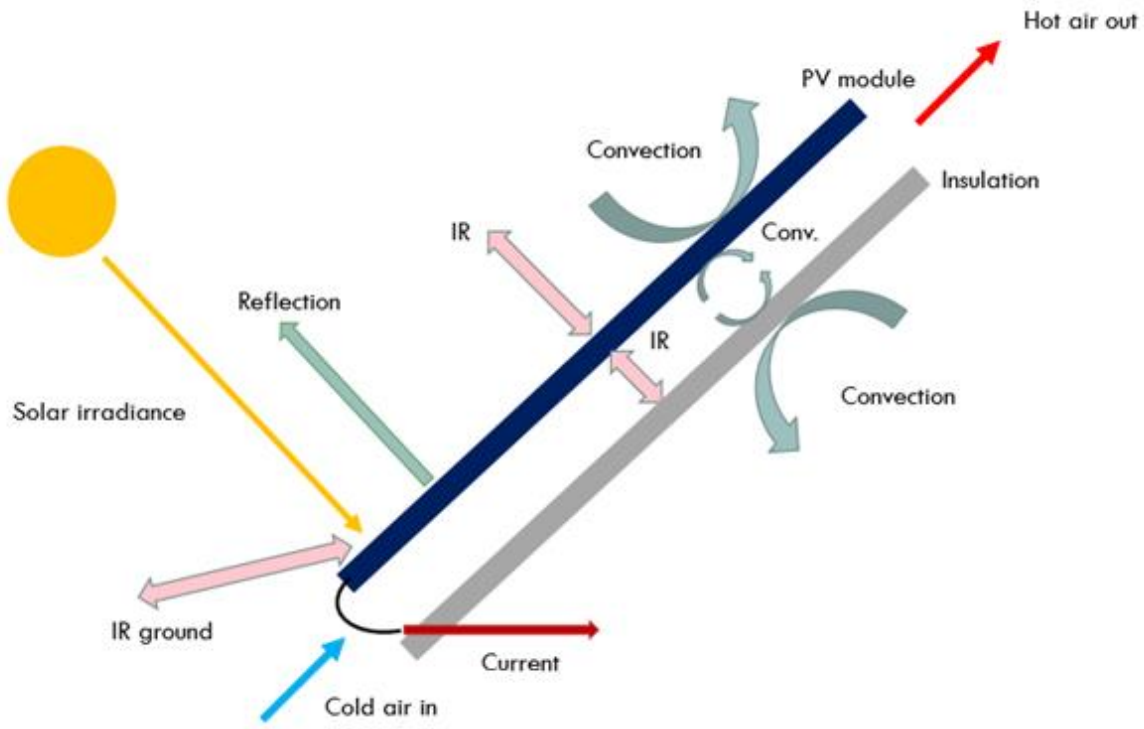

Figure 18. Heat balance of PVT air system [39]

3.2.1. PV cell absorption

The PV cells absorption is calculated by the formula:

$$\alpha_{PV}\tau_{gl}G \quad (1)$$

where α_{PV} is PV cell absorption, $\alpha_{PV} = 0.97$ τ_{gl} - glass transmittance, $\tau_{gl} = 0.93$, G – irradiance level.

3.2.2. IR heat exchange

3.2.2.1. IR radiation that is emitted from the sky

$$IR_{gl} = \sigma \cdot \epsilon_{gl} \cdot T_{gl}^4 \quad (2)$$

where σ is the Stefan-Boltzmann constant, ϵ_{gl} is the glass emissivity, $\epsilon_{gl} = 0.84$, T_{gl} is the glass absolute temperature.

3.2.2.2. IR radiation that is received from the sky

$$IR_{sky} = \sigma \cdot VF_{sky} \cdot T_{sky}^4 \quad (3)$$

where VF_{sky} is the sky view factor and the temperature of the sky is calculated as

$$T_{sky} = 0.05532 \cdot T_{amb}^{1.5} \quad (4)$$

where T_{amb} – ambient air temperature.

3.2.2.3. IR radiation that is received from the ground

$$IR_{gr} = \sigma \cdot \epsilon_{gr} \cdot VF_{gr} \cdot T_{gr}^4 \quad (5)$$

where ϵ_{gr} – ground emissivity, VF_{ground} is the ground view factor, T_{gr} is the ground absolute temperature.

3.2.2.4. IR heat exchange in the PV channel between back sheet and insulation

$$IR_{i1} = \frac{\sigma \cdot (T_{bs} + T_{pow}) \cdot (T_{bs}^2 + T_{pow}^2) \cdot (T_{bs} - T_{i1})}{1/\epsilon_{bs} + 1/\epsilon_i - 1} \quad (6)$$

where ϵ_{bs} is emissivity of the PV module back sheet, $\epsilon_{bs} = 0.84$, ϵ_i is emissivity of the insulation surface, $\epsilon_{bs} = 0.95$, T_{bs} is the absolute temperature of the back sheet surface, T_{i1} is the absolute temperature of the insolation surface.

3.2.3. Convectional heat exchange

3.2.3.1. Convectional heat exchange between the PV module and the ambient air

Because of the difference in the temperatures between the glass and ambient air the heat loss occurs.

$$CV_{gl} = h_w \cdot (T_{gl} - T_{amb}) \quad (7)$$

where h_w is the heat transfer coefficient that can be calculated as

$$h_w = 5.8 + 2.1 \cdot ws \tag{8}$$

where ws – wind speed

3.2.3.1. Convectional heat exchange between the ambient air and the channel walls.

The convection of the back sheet of the PV module is calculated with following equation:

$$CV_{bs} = h_{conv} \cdot (T_{bs} - T_{air}) \tag{9}$$

The convection of the front sheet is

$$CV_{pw} = h_{conv} \cdot (T_{pw} - T_{air}) \tag{10}$$

where T_{air} is the temperature in the air channel, h_{conv} is the heat exchange rate and calculated by the equation:

$$h_{conv} = \frac{k_m}{D_h} \cdot Nu \tag{11}$$

where k_m is thermal conductivity of the air, Nu is the Nusselt number, D_h is the hydraulic diameter of the air channel with width (W) and the thickness (d): $D_h = \frac{2Wd}{(W+d)}$, Nu is is the ratio of convective to conductive heat transfer across the boundary.

For forced convection, the Nusselt number is generally a function of the Reynolds number and the Prandtl number, or *Nu =f(Re,Pr)*. For being familiar with the type of the flow (laminar or turbulent), the Reynolds number has to be calculated:

$$Re = \rho_m \cdot \vartheta_{air} \cdot D_h / \mu_m \quad (12)$$

where ρ_m - is the density of the air in the channel, μ_m is the dynamic viscosity of the air, ϑ_{air} is the flow speed. In case if $Re \leq 3000$ the flow is laminar and if $Re > 3000$ it is turbulent. Further calculations depend on the result of the Reynolds number.

3.2.4. Heat balance of each layer in the PVT air system

The model divides such a system into layers with the independent variable z in the direction of the moving air that is depicted in Figure 19.

Such assumptions were conducted by the author for simlifying calculation for heat balance:

- cell, glass and back sheet have uniform temperatures;
- the polyolefin from each side is divided in half and one part is added to the cells and the others to the glass and back sheet;
- temperature distribution over the PV module sidewise is uniform.

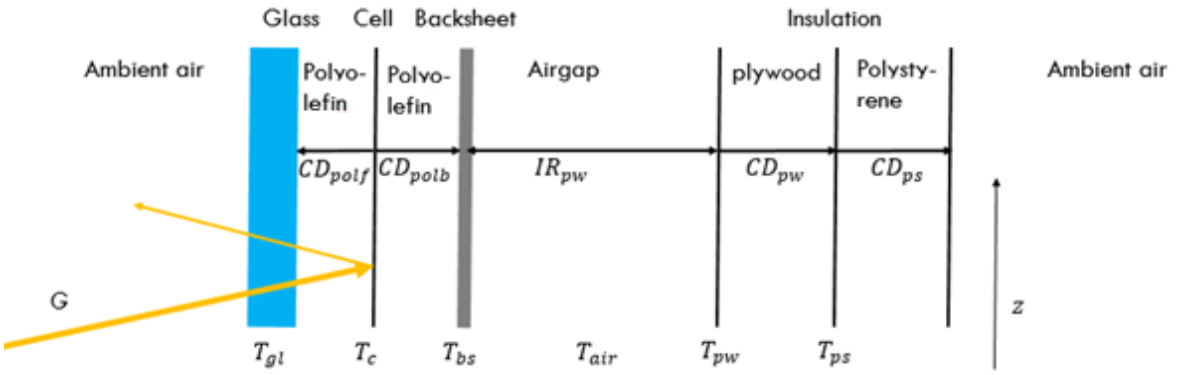

Figure 19. The structure of each layer of the PVT air system [39]

The heat balance is described in six differential equation:

- Airgap:

$$\frac{\partial T_{air}}{\partial z} = \frac{hconv}{v_{air} d \rho_a c_a} \left(T_{bs} + T_{pw} - 2T_{air}\right) \quad (13)$$

where d is the thickness of the air channel, ρ_a is the density of the air in the channel, c_a is a specific heat of the air in the channel and z is the axis with the direction of the air flow and change in air temperature in the channel.

- Insulation with polystyrene layer (insolation layer 0):

$$\frac{m_{ps}c_i}{2}\left(\frac{\partial T_{ps}}{\partial t}+\frac{\partial T_{in}}{\partial t}\right)=CD_{pw}-CD_{ps} \tag{14}$$

where m_{ps}, c_{pl} are mass and specific heat capacity of polystyrene and CD_{ps} is actually equal to CV_{ps} and T_{in} is temperature indoors.

- Insulation with plywood layer (insolation layer 1):

$$\frac{m_{pw}c_{pw}}{2}\left(\frac{\partial T_{pw}}{\partial t}+\frac{\partial T_{ps}}{\partial t}\right)=-CD_{ps}+IR_{pw}-CV_{pw} \tag{15}$$

where m_{pw}, m_{ps}, are mass of plywood and polystyrene and c_{pw}, c_{ps} are specific heat capacity of plywood and polystyrene.

- Back sheet:

$$\left(m_{bs}c_{bs}+\frac{m_{polb}c_{pol}}{2}\right)\frac{\partial T_{bs}}{\partial t}=-IR_{pw}+CD_{polb}-CV_{bs} \tag{16}$$

where m_{bs}, m_{polb} are mass of metal sheet and polyolefin and c_{bs}, c_{pol} are specific heat capacity of metal sheet and polyolefin.

- Cell:

$$\left(m_{\mathrm{c}}c_{\mathrm{c}}+\frac{m_{polb}c_{pol}+m_{polf}c_{pol}}{2}\right)\frac{\partial T_c}{\partial t}=-CD_{polb}+\alpha_{pv}\tau_{gl}G-PV-CD_{polf} \tag{17}$$

where m_c is mass of cells, c_c is specific heat capacity of cell and T_c is the temperature of cell and PV is heat energy which is driven away by the current.

- Front glass:

$$\left(m_{gl}c_{gl} + \frac{m_{polf}c_{pol}}{2}\right)\frac{\partial T_{gl}}{\partial t} = CD_{polf} + \alpha_{gl}G - CV_{gl} - IR_{gl} + IR_{sky} + IR_{gr} \quad (18)$$

where m_{gl} is mass of glass, c_{gl} is a specific heat capacity of glass and α_{gl} is an absorption of glass.

Initial conditions: $T_{ps}^{t=0}$=*C1*, $T_{pw}^{t=0}$=*C2*, $T_{bs}^{t=0}$=*C3*, $T_{air}^{t=0}$=*C4*, $T_{tc}^{t=0}$=*C5*, $T_{gl}^{t=0}$=*C6*

where *C1*-*C6* are constants.

We used weather data (solar radiation, humidity and temperature) for Estonia, Tallinn, which was measured in the period from 1st June to the 30th of September.

3.3. Simulation of PV output power

Perez model [40] have been used in order to estimate the electricity production, which requires such parameters as horizontal global irradiance and diffused irradiance.

PV output power was calculated as follows:

$$P_{mod} = P_{max}\, G'(1 + F_0 logG' + F_1 logG' + \gamma t') \quad (19)$$

where P_{max} is maximum power of the module in standard conditions, γ is a temperature coefficient of maximum power, $G'=G/1000$, $t'=t_{mod}-25$ (where t_{mod} is a temperature of the modules) and F_0=-0,01228, F_1=-0,01681 are coefficients for crystalline silicon cells.

3.4. Simulation of heater power

The heater power can be calculated as following:

$$P_{heater} = \dot{m} \cdot c_p \cdot (t_{s.p.} - t_{inlet}) \quad (20)$$

where $\dot{m}$ is air mass flow rate, c_p is specific heat of air, $t_{s.p.}$ is set point temperature in the drying chamber and t_{inlet} is temperature of the inlet heater air.

3.5. Simulation of the batteries

In order to increase self-consumption of the dryer, we included the batteries to the system.

For calculation of the batteries charge level, we used following equation:

$$E_{bat_i} = E_{bat_{(i-1)}} + \eta \cdot (P_{PV_i}\tau - P_{C_i}\tau) \quad (21)$$

where $E_{bat_{(i-1)}}$ is the energy charge level of the battery for a previous hour *(i-1)*, τ is a time, η is efficiency of batteries charging cycle (if $(P_{PV_i}\tau - P_{C_i}\tau) > 0$ then η=0.8, if $(P_{PV_i}\tau - P_{C_i}\tau) < 0$ then $\eta=1$).

The electrical capacity of the batteries was calculated as a maximum number of the vector E_{bat}.

3.6. Simulation of temperature and humidity in the drying chamber

The relative humidity and the temperature of the air are very important factors in the product dehydration. The temperature drops before each of the trays due to the heat losses through the walls of the drying chamber and evaporation of the moisture. Following equations (22)-(25) describe the heat balance for each tray and were used for simulation of the hourly actual temperature:

$$\Delta Q_{i,j} = Q_{ev_{i,j-1}} + Q_{losses_{i,j}} \quad (22)$$

where the subscript $i = 1 \ldots n$ defines the hour number, the subscript $j = 0$ defines parameters of the outside air and $j = 1 \ldots m$ – parameters of the air for each tray, $Q_{ev_{i.j-1}}$ is the energy needed for moisture evaporation, $Q_{losses_{i,j}}$ is the heat losses through the walls, $\Delta Q_{i,j}$ - heat rejection from the air.

Heat balance of the dryer is depicted in Figure 20.

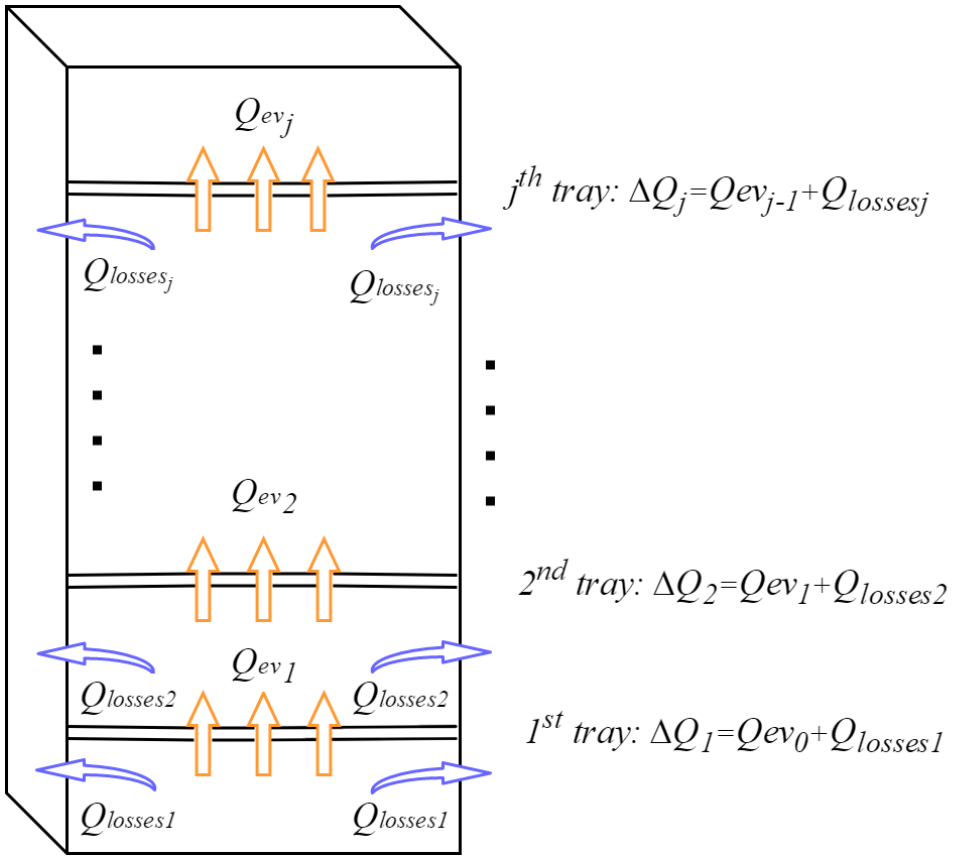

Figure 20. Heat balance in the dryer

Heat rejection is calculated as following:

$$\Delta Q_{i,j} = c \cdot \dot{m}_{a_i} \cdot \left(t_{i,j} - t_{i,j+1}\right) \cdot \tau \qquad (23)$$

where c is the heat capacity of the air (1.05 kJ/(kg·K)), $\dot{m}_{a_{i,j}}$ is the air mass flow rate, $t_{i,j}$ is the air temperature, τ is the time.

$$Q_{ev_{i,j}} = L \cdot \dot{m}_{ev_{i,j}} \cdot \tau \quad (24)$$

where L is the latent heat of the water, which is 2264.76 kJ/kg, $\dot{m}_{ev_{i,j}}$ is the moisture evaporation rate from the tray that was calculated with equation (36).

$$Q_{losses_{i,j}} = \frac{(t_{i,j} - t_0)}{\frac{\delta_1}{\lambda_1} + \frac{\delta_2}{\lambda_2}} \cdot S_j \cdot \tau \quad (25)$$

where t_0 is the outside temperature, δ_1 is the material layer thickness of the extruded polystyrene, δ_1 = 0.03 m, δ_2 is the material layer thickness of the plywood, δ_2 = 0.015 m, λ_1, λ_2 are the thermal conductivity of the extruded polystyrene and plywood respectively, λ_1 = 0.03 W/(m·K), λ_2 = 0.16 W/(m·K), S_j is the walls' area.

Based on the equations (22)-(23) the hourly temperature for each tray was calculated:

$$t_{i,j+1} = t_{i,j} - \frac{Q_{ev_{i,j}} + Q_{losses_{i,j}}}{c \cdot \dot{m}_{a_i}} \quad (26)$$

The relative humidity is the ratio of the water vapor's partial pressure to the saturation vapor pressure. Since the temperature changes after heating and after each tray, it affects the saturation vapor pressure. In addition, evaporation from each tray causes the change in the partial pressure of water vapor. Therefore, relative humidity is recalculated after heater and each tray taking into account temperature drop and additional evaporation. Following equations (27)-(30) were used for the simulation of relative humidity with initial conditions for outside air.

Magnus-Tetens equation is used for the calculation of saturated vapor pressure [41]:

$$p_{S_{i,j}} = 6.112 \cdot exp\left(\frac{17.67 \cdot t_{i,j}}{t_{i,j} + 243.5}\right) \quad (27)$$

The ideal gas equation was applied to calculate absolute humidity:

$$Ah_{i,j} = \frac{m_{w\,i,j}}{V_{i,j}} = \frac{M \cdot p_{S\,i,j}}{R \cdot t_{i,j}} \frac{Rh_{i,j}}{100} \tag{28}$$

where $m_{w\,i,j}$ is the actual water mass in the air, $V_{i,j}$ is the air volume, *M* is the molecular weight of water, which is 18.02 g/mol, R is the ideal gas constant, which is 0.08314 $\frac{\mathrm{m^3hPa}}{\mathrm{mol \cdot K}}$, $Rh_{i,j}$ is the air relative humidity.

Recalculation of absolute humidity taking into account moisture's evaporation rate from the tray:

$$Ah_{i,j+1} = Ah_{i,j} + \dot{m}_{ev\,i,j} \cdot \tau \tag{29}$$

$\dot{m}_{ev\,i,0} = 0$, because there is not additional evaporations after heater.

Equation for recalculation of relative humidity for new temperature and absolute humidity was expressed from the equation:

$$Rh_{i,j+1} = \frac{Ah_{i,j+1} R \cdot t_{i,j+1}\, 100}{M \cdot p_{S\,i,j+1}} \tag{30}$$

3.7. Drying kinetics simulation

Drying kinetics of apples were simulated by using empirical mass transfer model, involving a characteristic parameter (drying constant), as a function of process variables [42]. Samples dimensions, humidity, temperature and velocity were taken into account in the simulation.

The initial and final moisture contents of the apples are 80% and 24% of the total mass taken from the Ref. [43]. The moisture transfer within the fruits was described with the linear differential equation:

$$-\frac{dX_{S\,i,j}}{d\tau} = k_{M\,i,j} \cdot (X_{S\,i,j} - X_{SE\,i,j}) \tag{31}$$

where $k_{M_{i,j}}$ *i*s the drying constant, $X_{S_{i,j}}$ *i*s the material moisture content, $X_{SE_{i,j}}$ is the equilibrium material moisture content.

The equilibrium moisture content of products is calculated by well-known GAB equation [44]:

$$X_{SE_{i,j}} = X_M \cdot C_{i,j} \cdot \frac{K_{i,j} \cdot a_{W_{i,j}}}{\left(1 - K_{i,j} \cdot a_{W_{i,j}}\right)\left(1 - K_{i,j} \cdot a_{W_{i,j}} + C_{i,j} \cdot K_{i,j} \cdot a_{W_{i,j}}\right)} \quad (32)$$

where X_M, $C_{i,j}$ and $K_{i,j}$ are coefficients which characterize sorption properties of material, $a_{W_{i,j}}$ is the water activity of surrounding air, $a_{W_{i,j}} = Rh_{i,j}/100$.

Coefficients $C_{i,j}$ and $K_{i,j}$ are related to temperatures and can be calculated as follows:

$$C_{i,j} = C_0 \cdot exp(\Delta H_C/(t_{i,j} + 273.15)) \quad (33)$$

$$K_{i,j} = K_0 \cdot exp(\Delta H_K/(t_{i,j} + 273.15)) \quad (34)$$

where ΔH_C and ΔH_K are functions of water heat of sorption and water vapor heat of condensation. Table 2 shows the values of ΔH_C, ΔH_K, C_0 and K_0, which were fitted by the regression analysis for the GAB equation using experimental data of drying apples from Ref. [42].

Table 2. Coefficients fitted by regression analysis.

X_M, kg/kg db	C_0	$\Delta H_C(t)$	K_0	$\Delta H_K(t)$
0.945	0.162	8.554	0.06	805.977

The following empirical equation takes into account process variables (dimensions, humidity, temperature and velocity) for improving the goodness of the model:

$$k_M = k_0 \cdot d_p^{k_1} \cdot t^{k_2} \cdot \vartheta^{k_3} \cdot {a_w}^{k_4} \quad (35)$$

where d_p is the particle dimension, which was taken 0.028 m, ϑ is the air velocity.

Table 3.The empirical coefficients k_0, k_1, k_2, k_3, k_4 were taken from Ref. *[42]*:

k_0, h^{-1}	k_1	k_2	k_3	k_4
$1.3 \cdot 10^{-6}$	-1.58	1.62	0.19	-0.034

The water evaporation rate was calculated using the following equation:

$$\dot{m}_{ev_{i,j}} = X_{S_{i,j}} - X_{S_{i,j-1}} \quad (36)$$

4. Result and discussion

In order to find the optimum configuration of the drying chamber, we performed the simulations of the drying process using various numbers and dimensions of trays in the drying chamber for one-directional and bidirectional regimes.

Simulations were conducted for set point temperature of 60˚C and different configurations of the drying chamber. The maximum possible number of trays was limited by the temperature (not lower than 30 ˚C) and relative humidity (not higher than 85%) at the level of last tray. The air mass flow rate was constant 0.5 m^3/s. Product load on the trays was different in order to provide equal cross section for air flow and equal conditions for drying with air speed of 2 m/s for different trays configuration.

The Table 4 shows that the smaller tray's area the more trays it is possible to have in a stack. There is good correlation between mass of raw apples and surface on trays covered with product. The larger surface the larger amount of apples to be dried. However, it was impossible to provide the equal surface covered with product in all cases as product load determined by the air speed. Thus, for estimation of the best configuration we decided to compare the mass of apples divided by the surface on trays covered with product. And this indicator is approximately equal for all tray's areas in case of one-directional air flow. Therefore, tray's configuration does not affect the mass of apples for one-directional air flow.

Table 4. The results of simulations for one-directional air flow

Tray's area, m^2	0.5	1	2	3
Maximum possible trays in a stack	23	9	4	3
Total trays' area, m^2	11.5	9	8	9
Product load on trays, %	50	75	88	92
Surface on trays covered with product, m^2	5.75	6.75	7	8.25
Mass of raw apples to be dried in a season, kg	31640	36903	38855	45472
Mass of apples by surface covered with product, kg/m^2	5503	5467	5551	5512

The Table 5 shows that the mass of apples to be dried by surface on trays covered with product increases with increase of tray's area in case of bidirectional air flow. Comparing the mass of apples by surface on trays covered with product from the Table 4 and Table 5 it is possible to see that in case of bidirectional air flow it is larger. Also in case of bidirectional air flow it increases with trays' area increase. If tray's area is $3m^2$ mass of apples by surface on

trays covered with product is bigger by 30% comparing to 0.5m^2 tray's area. Therefore, tray's configuration affects the mass of apples and the larger tray's area the more product is dried.

Table 5. The results of simulations for bidirectional air flow

Tray's area, m^2	0.5	1	2	3
Maximum possible trays in a stack	23	9	4	3
Total trays' area, m^2	11.5	9	8	9
Product load on tray, %	50	75	88	92
Surface on trays covered with product, m^2	5.75	6.75	7	8.25
Mass of raw apples to be dried in a season, kg	32175	39866	48775	58473
Mass of apples by surface covered with product, kg/m^2	5596	5906	6968	7087

For further simulations, we have chosen tray's configuration with area of 1m^2 because this size of trays are convenient to handle. In addition, we decided to simulate bidirectional airflow. Because in this case the product is dried by batch (all trays in the same time) and the the amount of the fruits that can be dried in bidirectional regime is larger than in one-directional. Covered area by the product on trays is 70%. Results are simulated for Estonian climate conditions from the 1st of June to the 30th of September. System runs 24/7. The energy production has been simulated for the system with no product load. The energy of condensation in HRU was not taken in to account. Since the air mass flow rate was constant 0.5 m^3/s there was no regulation of the temperature in the drying chamber. Therefore, we assume that if the temperature was higher than set point temperature system did nothing. However, if the temperature was lower the air was heated by electrical heater.

Figure 21, Figure 22 and Figure 23 show the hourly heat production by the system for different set point temperatures. There are two areas on each figure. The area on bottom is amount of the heat that is produced by HRU and with/without PV channel (depending on the chosen mode) and the area on the top is heat produced by the heater. The bottom boundary of the heat from the HRU and with/without PV channel represents the ambient temperature during simulated period. The upper boundary of this area is the temperature before the heater. The upper boundary of the heat produced by heater is the set point temperature. Form these figures it is possible to observe that the higher set point temperature the more heat from electrical heater is required and consequently the more heat is recovered by HRU. Sometimes the temperature before the heater gets higher than set point temperature and the air with this temperature actually

goes for drying of apples. According to the Ref. [43] the drying temperature of the apples should not exceed 70˚C. From the graphs, we can see that temperature does not get higher than 70˚C.

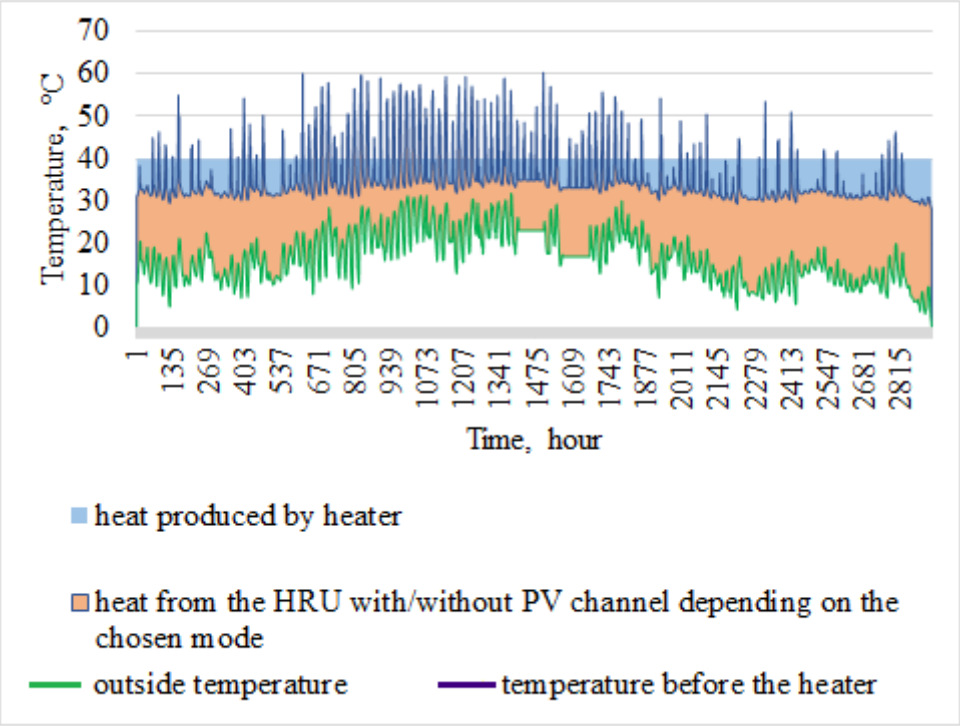

Figure 21. Structure of heat production with set p–oint temperature 40˚C

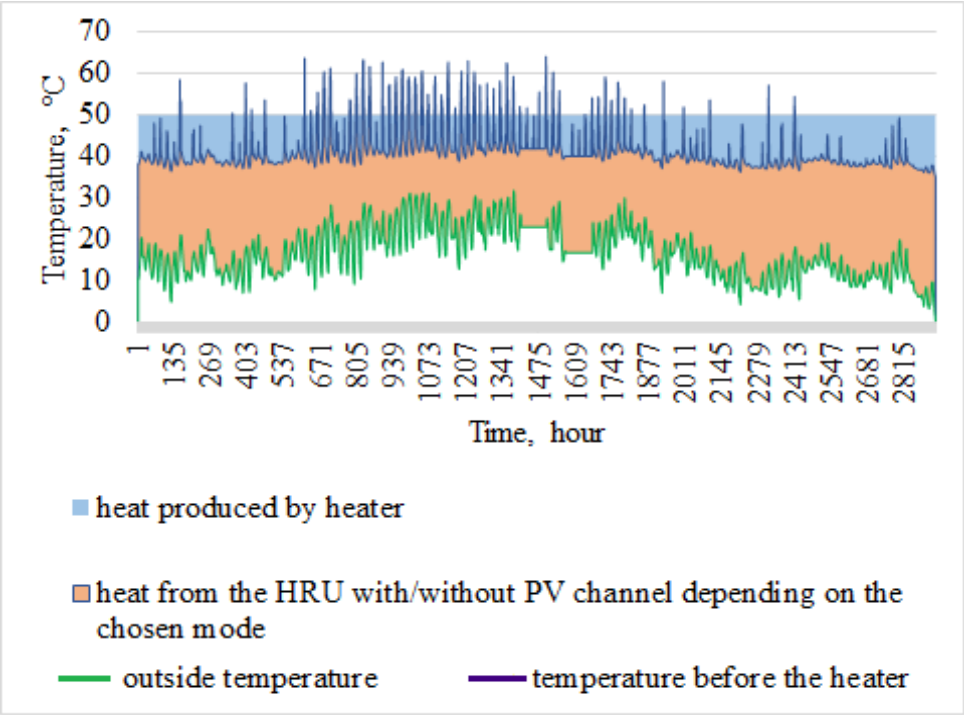

Figure 22. Structure of heat production with set point temperature 50˚C

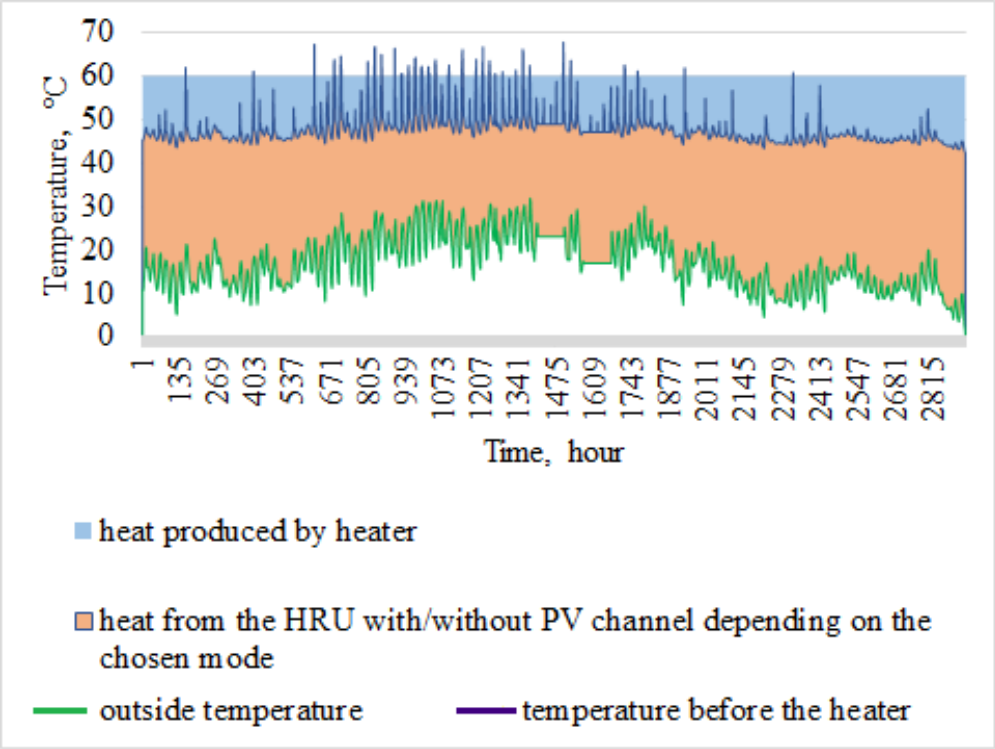

Figure 23. Structure of heat production with set point temperature 60˚C

Table 6 presents the main results of the system performance simulations for different set point temperatures in the drying chamber. From simulations we obtained the amount of energy needed to maintain desired set point temperature. The higher set point temperatures the more energy is required. Total produced heat energy is almost doubled for set point temperature 60˚C comparing with 40˚C as well as the mass of apples to be dried. The system requires significantly more energy from the grid for use by electrical heater with higher set point temperature. In addition, it becomes less autonomous. Coefficient of performance (COP) is ratio between the heat energy produced by the system to AC energy taken from the grid and shows how many heat energy is produced by one kWh taken from the grid. Higher COP leads to lower operation costs. In case of our system the lower set point temperature the higher COP.

Table 6. Results of simulations of system performance for different set point temperatures

Set point temperature	40˚C	50˚C	60˚C
Solar radiation collected by PV during the simulated period, kWh	40410		
Total produced heat energy, kWh	43898	60564	78040
Heater consumption, kWh	10727	16224	22159
AC from the grid, kWh	7653	13022	18842
Autonomous hours, h	1188	707	353
Hours in mode 1, h	706	523	375
Maximum AC power, kW	7.3	9.1	11
Maximum heater power, kW	7.3	9.1	11
Maximum charge power, kW	6.3	6.2	6.1
Battery capacity, kWh	45.9	39.1	29.1
Air flowrate, m^3/s	0.5	0.5	0.5
Mass of apples to be dried in a season, kg	21913	30425	39866
Coefficient of performance (COP)	5.74	4.65	4.14

Figure 24 shows Sankey diagram of energy balance for drying system providing constant set point temperature of 40˚C during a season. This is one of the common ways to present energy balance of the system. Sankey diagram is a type of flow diagram where the widths of the bands are proportional to the flow quantity. Each node has its name and a number that represents amount of energy in kWh. At the left side of the Sankey diagram there are energy inputs: solar radiation and AC electricity from the grid. Part of solar radiation is converted into electricity and heat energy. Large amount of solar irradiance is lost from PVT and this is because production of the heat by HRU. When HRU provides high temperatures of the air, BIPVT collectors cannot be cooled down significantly. Higher absorption of solar irradiance could be achieved by increasing of the fan speed. Electricity from the grid and PV panels is used by the fan and the electrical heater. Total produced heat is used in drying chamber and there are losses through the walls of drying chamber. Losses in pipes were not taken into account. After drying chamber exhaust air is released to environment through the HRU and part of heat is recovered.

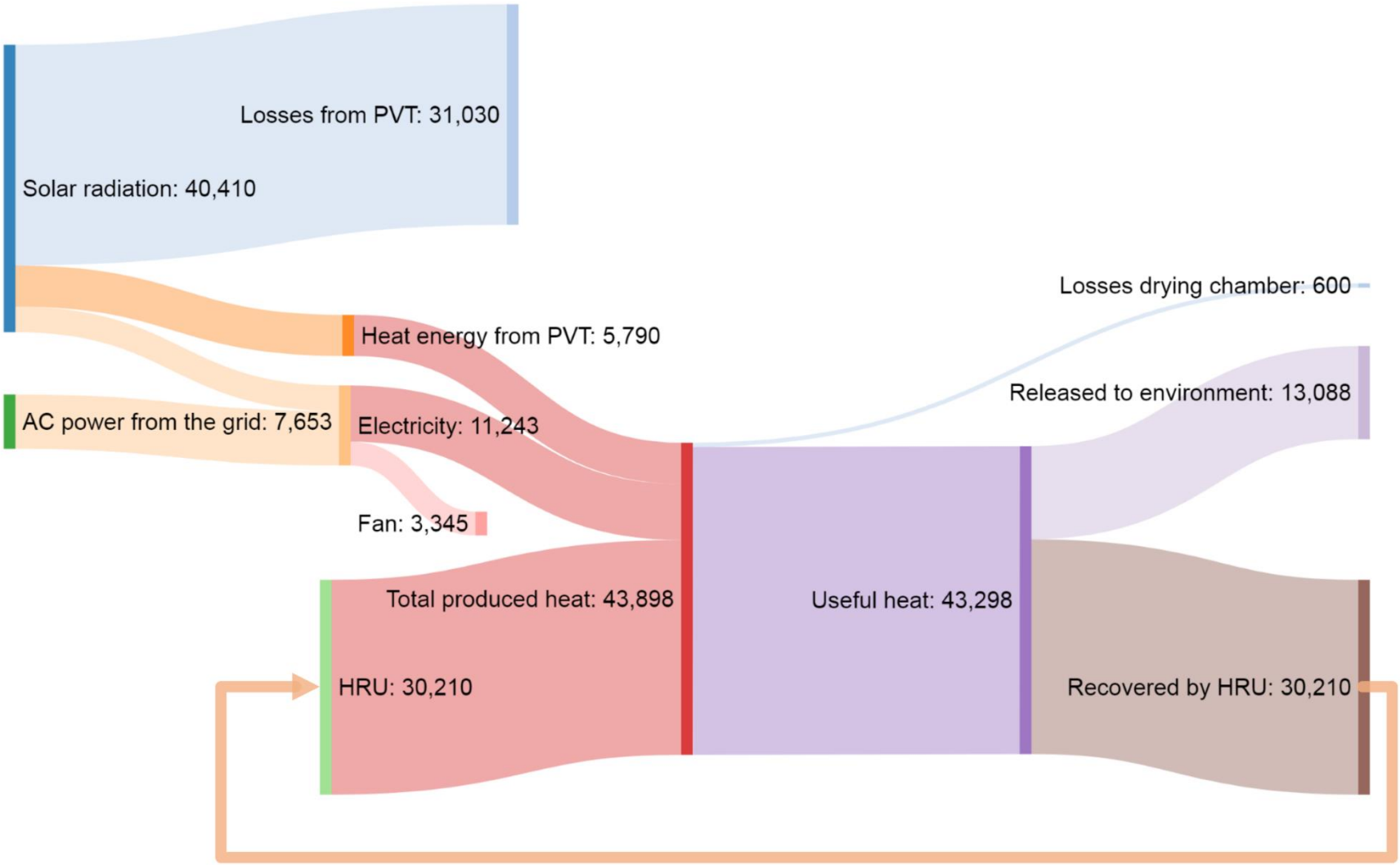

Figure 24. Sankey diagram of energy balance for drying system

5. Conclusion

We have simulated the performance of a solar drying system based on air type BIPVT collectors in the Estonian climate for period from the 1st of June to the 30th of September for different set point temperatures in the drying chamber; the amount of the apples to be dried depending on the drying chamber configurations, air flow directions and different set point temperatures in the drying chamber.

With one-directional air flow the difference of the mass of apples to be dried by surface covered with product is not significant for different tray's configuration. For instance, for all tray's configuration are about 5500 kg/m^2. In comparison for bidirectional air flow the mass of apples by surface covered with product gradually increases with tray's area increase. For the tray's areas 0.5 m^2 and 3 m^2 this indicators are 5596 kg/m^2 and 7087 kg/m^2 respectively. Bidirectional air flow has shown better results and it is more convenient in operation. Therefore, it was used for further simulation.

Solar radiation collected by PV during the simulated period is 40410 kWh. Total heat energy produced by the system is 43898 kWh, 60564 kWh and 78040 kWh for set point temperatures 40 ˚C, 50 ˚C and 60 ˚C respectively. The total mass of apples to be dried using produced amounts of heat energy are 21913, 30425 and 39866 kilograms. The specific energy consumption for drying of one kilogram of apples is about 2 kWh/kg.

The COP is higher in case when the set point temperature is 40 ˚C because lower temperature requires less energy from the grid. However, less product can be dried. We can see that food dehydration system with use of BIPVT technology can amplify the electrical energy taken from the grid by 4 up to 6 times depending on set point temperature. The system can run 40% of the time off grid.

The heat consumption under the loaded condition must be verified by further analysis.

Résumé

The purpose of this study is to simulate the performance of drying system based on hybrid BIPVT collectors working on different set point temperatures, to simulate the amount of apples to be dried.

The simulation has been conducted for a theoretical farmhouse covered with air type BIPVT collectors with total area of 70 m^2 and nominal PV power of 9 kW. BIPVT collectors are standing seam metal sheet integrated PV cells with air gap organized under PV modules. Such type of collectors allow production of electricity by PV cells and heat by running of the air through the PVT channel. There are two modes in the system and each of them used for specific conditions. The first mode is used in order to heat up air in the PVT channel. Otherwise, in the second mode the air bypasses the PVT channel in order to avoid its cooling. The drying system also comprised fan, heater, HRU and electrical batteries. The system had connection to the grid for providing continuous 24/7 operation. Simulation has been conducted hourly for Estonian climate conditions from 1st June till 30th September.

For simulation of collectors' thermal output the dynamic thermal model was used. Model includes six differential equations that were solved numerically. It takes into account infrared heat exchange between PV module, ground, sky and insulation layer, convectional heat exchange with ambient air and the air in PVT channel and heat which is driven away by current. Simulations were conducted for constant air flow (0.5 m^3/s) and HRU efficiency (70%). Heat production by the system was calculated without taking into account water condensation in HRU.

For simulations of drying kinetics of the apples, we used mathematical model that include air velocity, temperature, humidity and sample dimensions of the product. Calculations of air parameters were conducted for each tray level with taking into account heat losses through the walls and additional evaporations from previous trays that lead to temperature drop and humidity rise.

According to the simulated results, the bidirectional air flow is more effective. Consequently, more apples can be dried and it is easier to operate and control the drying rate of the product. Total produced heat energy by the system is 43898 kWh for 40˚C, 60564 kWh for 50 ˚C and 78040 kWh for 60˚C of set point temperature in the drying chamber. Heat energy that is needed in order to dry one kilogram of apples is about 2 kWh/kg. Coefficient of performance of the system is 5.74, 4.65, and 4.14 for 40˚C, 50˚C and 60˚C set point temperature respectively. In case of our system the lower set point temperature, the higher COP.

Resümee

Käesoleva töö eesmärgiks on hoone katusele paigaldatud ehitisintegeeritud päikesepaneelide baasil loodud toiduainete kuivati teostatavuse analüüs. Simulatsioonid on tehtud 70 m^2 katusele, millele on paigaldatud 9 kW nominaalse võimsusega ehitisintegreeritud päikeseelektri süsteem. Sooja õhu tootmine toimub päikesepaneelide jääksoojuse arvelt paneelide all oleva õhukanali kaudu.

Simulatsioonides arvestasime, et vastavalt päikesekiirguse hulgale võib süsteem töötada kahes režiimis. Esimeses töörežiimis toimub kuivatusõhu eelsoojendamine soojustagastis väljuva õhu soojusenergia arvel ning järgnev soojenemine toimub päikesepaneelide all olevas õhukanalis. Samuti on võimalik süsteemi lisada soojusenergiat elektrilise küttekeha abil. Teist režiimi kasutatakse öösel, kui päikesepaneelide all oleva õhukanali kasutamine ei ole infrapuna jahutusefekti tõttu mõttekas. Sellisel juhul toimub kuivatusõhu soojendamine ainult soojusvaheti ja elektrilise kütekeha abil. Küttekeha elektrienergiaga varustamine toimub kas päevasel ajal akudesse salvestatud päikeseelektri või võrgust ostetud elektrienergia arvel, mis tagab süsteemile 24/7 toimimise.

Ehitisintegreeritud päikesepaneelide soojusenergia tootluse modelleerimiseks kasutasime dünaamilist mudelit, mis koosneb kuuest diferentsiaalvõrrandist. Soojuslik mudel võtab arvesse päikesepaneelide soojusenergia vahetuse keskkonnaga nii infrapuna kiirguse kui konvektsiooni kaudu. Võrrandite lahenduse tuletasime kasutades numbrilisi meetodeid. Simulatsioonides arvestasime konstantse kuivatusõhu vooluhulgaga 0.5 m3/s. Soojustagasti keskmiseks efektiivsuseks võtsime 70% ning me ei arvestanud aurustumisest ning kondenseerumisest tekkivate soojusülekannetega.

Üheks simulatsioonide eesmärgiks oli välja arvutada õunte hulk, mida on teoreetiliselt võimalik antud süsteemiga vegetatsiooniperioodi jooksul kuivatada. Selleks kasutasime kuivamise kineetilist mudelit, mis võtab arvesse kuivatusõhu liikumise kiiruse, niiskuse taseme, kuivatusõhu temperatuuri ning kuivatatavate saaduste mõõtmed. Simulatsioonides võtsime arvesse ka selle, et õhu parameetrid kuivatuskambris muutuvad ruumiliselt pikki õhu liikumise suunda.

Süsteemi teostatavuse analüüsiks viisime läbi simulatsioonid tunniajalise sammuga perioodil 1.juuni kuni 30.september Eesti klimaatiliste tingimuste baasil. Simulatsioonide tulemused näitasid, et kuivati efektiivsuse suurendamiseks peaks iga tund kuivatusõhu suunda kuivatuskambris muutma. Samuti võimaldab muutuva õhuvoolu suunaga režiim kuivatusagregaati lihtsamini opereerida. Analüüsitud perioodi jooksul oli simulatsioonides toodetud soojusenergia hulk erinevatel kuivatustemperatuuridel 43898 kWh (40˚C), 60564 kWh (50 ˚C) ning 78040 kWh (60˚C). Erisoojushulk, mis on tarvis 1 kg õunte kuivatamiseks oli 2 kWh. Süsteemi energeetiline kasutegur võrgust ostetud elektrienergia suhtes oli erinevatel kuivatustemperatuuridel 5.74 (40˚C), 4.65 (50 ˚C), ja 4.14 (60˚C).

Literature review

[1] . T. Chow, "A review on photovoltaic thermal hybrid solar technology," *Appl Energy,* p. 79, 2010.

[2] M. S. Tushar and A. S. Dhoble, "A review on recent advancements in photovoltaic thermal techniques," *Renewable and Sustainable Energy Reviews,* p. 645–672, 2017.

[3] J. Konnova, "Solar technologies as an alternative sourse of energy," Electrical systems for buildings , Toronto, 2014.

[4] Y. Tripanagnostopoulos, T. Nousia, M. Souliotis and P. Yianoulis , "Hybrid photovoltaic/thermal solar systems," *Solar Energy,* vol. 72, no. 3, pp. 217-234, March 2002.

[5] Y. Kemmoku, T. Egami, M. Hiramatsu, Y. Miyazaki and K. Araki, "Modeling of Module Temperature of a Concentrator PV System," in *19th EU-PVSEC*, 2004.

[6] L. S. David, B. U. Natko and J. K. Zoltan, "Development of High Efficiency Hybrid PV-Thermal Modules," *29th IEEE Photovoltaic Specialists Conference,* pp. 1660 - 1663, 2002.

[7] S. Jian and S. Mingheng, "Numerical Simulation of Electric-Thermal Performance of A Solar Concentrating Photovoltaic/Thermal System," *IJSRD IEEE,* pp. 1-4, 2009.

[8] F. Huide, Z. Xuxin, M. Lei, Z. Tao, W. Qixing and S. Hongyuan, "A comparative study on three types of solar utilization technologies for buildings: Photovoltaic, solar thermal and hybrid photovoltaic/thermal systems," *Energy Conversion and Management,* p. 1–13, 15 May 2017.

[9] M. Hajiji, S. E. Naimi, B. Hajji and M. L. El Hafyani, "A numerical modeling of hybrid photovoltaic/thermal (PV/T) collector," *ICM,* pp. 152 - 155, 2014.

[10] S. Solanki, S. Dubey and A. Tiwari, "Indoor simulation and testing of photovoltaic thermal (PV/T) air collectors," *Appl. Energy,* vol. 11, no. 86, p. 2421–2428, 2009.

[11] M. A. Husan and K. Sumathy, "Photovoltaic Thermal Module Concepts and Their Performance Analysis: review," *Renewable and Sustainable Energy review,* vol. 14(7), pp. 1845-1859, 2010.

[12] C. Hachem, A. Athienitis and P. Fazio, "Design of Roofs for Increased Solar Potential BIPV/T Systems and Their Applications to Housing Units," *ASHRAE annual conference,* June, 2012.

[13] K. Vats and G. Tiwari, "erformance Evaluation of a Building Integrated Semitransparent Photovoltaic Thermal System for Roof and Facade," *Energy and Buildings,* no. 45, pp. 211-218, 2007.

[14] O. Zogou and H. Stapountzis, "Flow and Heat Transfer Inside A PV/T Collector for Building Application," *Applied Energy,* no. 91(1), pp. 103-115, 2012.

[15] P. G. Charalambous, G. G. Maidment, S. A. Kalogirou and K. Yiakoumetti, "Photovoltaic Thermal (PV/T) Collectors: A review," *Applied Thermal Engineering,* no. 27(2-3), pp. 275-286, 2007.

[16] R. Daghigh, A. Ibrahim, G. L. Jin, M. H. Ruslan and K. Sopian, "Predicting the Performance of Amorphous and Crystalline Silicon Based Photovoltaic Solar Thermal Collectors," *Energy conversion and Management,* no. 52(3), pp. 1741-1747, 2011.

[17] S. Bambrook and A. Sproul, "Maximizing The Energy Output of A PVT Air System," *Solar Energy,* no. 86(6), pp. 1857-1871, 2012.

[18] C. Cools, R. Gicquel, D. Mayer, L. Vandaele, P. Wouters, G. Barth, R. Digel, C. Twerdy, M. Chantant and J. M. Servant, The Passys Test Cells, Brussels: BBRI, May 1990.

[19] F. J. Crick, A. Wilshaw, N. M. Pearsall, K. Hynes, M. Shaw and G. Young, "Photovoltaic ventilated facade: system investigation and characterization," in *14th EPSEC,* Barcelona, 1997.

[20] A. Sharma, C. Chen and N. V. Lan, "Solar-energy drying systems: A review," *Renewable and Sustainable Energy Reviews,* no. 13, pp. 1185-1210, 2009.

[21] A. Leon, S. Kumar and S. Bhattacharya, "A comprehensive procedure for performance evaluation of solar food dryers," *Renewable and Sustainable Energy Reviews,* vol. 6, pp. 367-393, 2002.

[22] I. Farcas, "Solar drying," *Stewart Postharvest Review,* vol. 2, no. 9, pp. 2-8, 2008.

[23] M. Hamid, B. Ghobadian, S. Minaei and M. Khoshtaghaza, "Saffron Drying with a Heat Pump–Assisted Hybrid Photovoltaic–Thermal Solar Dryer," *Drying Technology,* pp. 560-566, May 2012.

[24] S. Nayak, Z. Naaz, P. Yadav and R. Chaudhary, "Economic Analysis of Hybrid Photovoltaic-Thermal (PVT) Integrated Solar Dryer," *International Journal of Engineering Inventions,* vol. 1, no. 11 , pp. 21-27, December 2012.

[25] H. Mortezapour, B. Ghobadian, M. H. Khoshtaghaza and S. Minaei, "Performance Analysis of a Two-way Hybrid Photovoltaic/Thermal Solar Collector," *Agriculture Scince Technology* , no. 14, pp. 767-780, 2012.

[26] C. Ratti and A. S. Mujumdar, "Solar drying of foods: modelling and numerical simulation.," *Solar energy,* no. 60, p. 151–157, 1997.

[27] T. Murthy and B. Manohar , " Microwave-drying of mango ginger (Curcuma amada Roxb): prediction of drying kinetics by mathematical modeling and artificial neural network," *Food Scince Technology,* vol. 6, no. 47, pp. 1229-1236, 2012.

[28] Z. Erbay and F. Icier , "A review of thin-layer drying of foods: theory, modeling, and experimental results.," *Food Science ,* vol. 5, no. 50, p. 441–464, 2010.

[29] E. Meisami-asl, S. Rafiee, A. Keyhani and . A. Tabatabaeefar , "Determination of suitable thin layer drying curve model for apple slices," *Plant Omics Journal ,* pp. 103-108, 2010.

[30] O. Yaldız, C. Ertekin and H. I. Uzun , "Mathematical modeling of thin layer solar drying of Sultana grapes," *Energy,* p. 457– 465, 2001.

[31] A. Yagcioglu, A. Degirmencioglu and F. Cagatay , "Drying characteristic of laurel leaves under different," in *7th international congress on agricultural mechanization*, Adana, Turkey, 1999.

[32] C. L. Hii, C. L. Law and M. Cloke, "Modeling using a new thin layer drying model and product quality of cocoa," *Journal of Food Engineering,* no. 90, p. 191–198, 2009.

[33] A. Midilli and H. Kucuk, "Mathematical modeling of thin layer drying of pistachio by using solar energy.," *Energy Conversion and Management,* vol. 7, no. 44, p. 1111–1122, 2003.

[34] M. Aghbashlo, M. H. Kianmehr, S. Khani and M. Ghasemi, "Mathematical modelling of thin-layer drying of carrot," *International Agrophysics,* vol. 4, no. 23, p. 313–317, 2009.

[35] E. K. Akpinar, "Determination of suitable thin-layer drying curve model for some vegetables and fruits," *Food Engr,* no. 73, pp. 75-84, 2006.

[36] M. Zarein , S. Samadi and G. Barat , "Kinetic drying and mathematical modeling of apple slices on dehydration process," *Food Process Technology,* vol. 4, no. 7, pp. 1-4, 2013.

[37] E. Meisami-asl and S. Rafiee, "Mathematical modeling of kinetics of thin layer drying of Apples," *Agric Engr,* no. 6, pp. 1-10, 2009.

[38] S. Timoumi, D. Mihoubi and F. Zagrouba, "Simulation model for a solar drying process," *Desalination,* no. 168, pp. 111-115, 2004.

[39] A. Jagomagi, "Thermal model of building integrated air type photovoltaic-thermal system under varying conditions," *32th European Photovoltaic Solar Energy Conference and Exhibition*, pp. 2740-2745, 2016.

[40] R. Perez, R. Seals, P. Ineichen, R. Stewart and D. Menicucci, "A NEW SIMPLIFIED VERSION OF THE PEREZ DIFFUSE IRRADIANCE MODEL FOR TILTED SURFACES," *Solar Energy,* vol. 3, no. 39, pp. 221-231, 1987.

[41] D. Bolton, "Computation of equivalent potential temperature," *American Metrological Society,* pp. 1046-1053, 1980.

[42] C. T. Kiranoudis, E. Tsami, Z. B. Maroulis and D. Marinos-Kouris, "Drying kinetics of some fruits," *Drying Technology,* pp. 1399-1418, 1997.

[43] M. A. Aravindh and A. Sreekumar, "Solar Drying—A Sustainable Way of Food Processing," in *Green Energy and Technology*, "Springer", 2015, pp. 27-46.

[44] J. Blahovec and S. Yanniotis, "GAB Generalized Equation for Sorption Phenomena," *Food Bioprocess Technol*, pp. 82-90, 2008.

[45] A. A., "Design of Advance solar Homes Aimed at Net-Zero Annual Energy Consumption in Canada," *NSERC Solar Buildings Research Network*, 2007.

[46] K. Jin-Hee, A. Jong-Gwon and K. Jun-Tae, "Demonstration of the Performance of an Air-Type Photovoltaic Thermal (PVT) System Coupled with a Heat-Recovery Ventilator," *Energies*, pp. 1-15, 2016.

[47] S. Nayak, Z. Naaz, Y. Pushpendra and R. Chaudhary, "Economic Analysis of Hybrid Photovoltaic-Thermal (PVT) Integrated Solar Dryer," *International Journal of Engineering Inventions*, pp. 21-27, 2012.

[48] M. Azharul Karim and M. N. A. Hawlader , "Mathematical modelling and experimental investigation of tropical fruits drying," *International Journal of Heat and Mass Transfer*, no. 48, p. 4914–4925, 2005.

Appendix 1

Acknowledgements

Foremost, I would like to express my sincere gratitude to my supervisor Andri Jagomagi for the continuous support, his patience, motivation and enthusiasm. His guidance helped me in all the time of research and writing of this thesis.

This study was supported by institutional research funding IUT (IUT 19-28) of the Estonian Ministry of Education and Research, and by the European Union through the European Regional Development Fund, projects TK141. This research has been done in collaboration with Roofit.solar Energy.

I am grateful to all the people who helped and contribute great ideas and advices, especially my husband Dmytro and lovely daughter Polina.

Finally, I am grateful to my parents for giving me the support of a lifetime.

Appendix 2

This work was performed at the following conference:

Photovoltaic Technical Conference (2017) with a poster entitled: “Simulations of building integrated photovoltaic-thermal food dehydrator with heat recovery”, Marseille, France.